Diffusion in channeled structures: Xenon in a crystalline sodalite

Benoit Palmieri and David Ronis
Department of Chemistry, McGill University, 801 Sherbrooke Ouest, Montréal, Québec, Canada H3A 2K6
(Received 18 February 2003; revised manuscript received 27 May 2003; published 27 October 2003)

The theory of Ronis and Vertenstein [J. Chem. Phys. **85**, 1628 (1986)] is used to calculate the permeability of xenon in Theta-1, a crystalline sodalite containing one-dimensional channels. The required time-correlation functions are obtained from numerical simulations performed using a small number of target crystal atoms. The dynamics of the target atoms reproduce those of the full crystal by the means of a generalized Langevin equation of motion. An approximate expression for the potential of mean force inside the crystal is derived. The plane average space-dependent diffusion coefficient $D(z)$ obeys the Smoluchowski prediction at infinite dilution. The permeability is reported and compared in detail with that obtained from transition state theory.

DOI: 10.1103/PhysRevE.68.046127 PACS number(s): 05.60.−k, 66.30.−h, 82.75.Jn, 05.10.Gg

I. INTRODUCTION

Understanding the diffusion of a guest component inside channeled structures (such as membrane channels, zeolites, and many silicates) has been a problem of interest for many years. Crystalline channeled structures have many applications in gas phase separation and are also widely used as catalysts in chemical reactions [1,2]. The diffusion of one or more guest components inside the crystal plays an important role in any of these applications. In this work, we develop a systematic approach that allows us to understand the diffusion process microscopically and calculate the macroscopic permeability of channeled structures to a guest component. Specifically, we will apply the theory to the diffusion of noble gases through Theta-1, a high silicate zeolite that shows a remarkable selectivity in catalysis applications [2] and could be a good candidate to study single-file diffusion [3,4].

Early theoretical calculations on channeled structures focused mainly on the heat of sorption [5,6]. These calculations were performed using a model potential for the guest-crystal interactions on a rigid lattice. Next, the diffusion in channels was studied through molecular dynamics (MD) simulation [7–9], where a diffusion coefficient was calculated from Einstein or Green-Kubo relations; cf. Eqs. (1.1) and (1.2) below. For high internal potential energy barriers, where barrier crossing events are rare, a common way to proceed was to determine a hopping rate constant using transition state theory [10–12].

In homogeneous systems, the diffusion coefficient D can be obtained using an Einstein relation,

$$D=\lim_{t\to\infty}\frac{\langle|\mathbf{r}(t)-\mathbf{r}(0)|^2\rangle}{6t}, \tag{1.1}$$

or equivalently by a Green-Kubo relation,

$$D=\frac{1}{3}\int_0^\infty dt\langle\mathbf{v}(t)\cdot\mathbf{v}(0)\rangle, \tag{1.2}$$

where $\mathbf{r}$ is the position of the guest, $\mathbf{v}$ is its velocity and $\langle\cdots\rangle$ denotes an equilibrium average. These last two equations are valid only for an uniform system, and imply a diffusion equation for the guest component of the form

$$\frac{\partial n(\mathbf{r},t)}{\partial t}=D\nabla^2 n(\mathbf{r},t), \tag{1.3}$$

where $n(\mathbf{r},t)$ is the number density of the guest.

In the second approach, transition state theory or one of its modified versions (cf. Refs. [10–12]) is used in a hopping model to calculate the hopping rate constants. Of course, transition state theory makes several assumptions, the key ones being that the motion closely follows the reaction coordinate and that there are no recrossings. This paper proposes an alternative and more general method that can also be used to verify the validity of transition state theory.

For bounded systems with large potential gradients, a more correct starting point is the generalized diffusion equation,

$$\frac{\partial n(\mathbf{r},t)}{\partial t}=\boldsymbol{\nabla}_{\mathbf{r}}\cdot\int d\mathbf{r}'\overleftrightarrow{L}(\mathbf{r}|\mathbf{r}')\cdot\boldsymbol{\nabla}_{\mathbf{r}'}\beta\mu(\mathbf{r}',t), \tag{1.4}$$

where $\mu(\mathbf{r},t)$ is the chemical potential and where the generalized Onsager diffusion coefficient,

$$\overleftrightarrow{L}(\mathbf{r}|\mathbf{r}')\equiv\int_0^\infty dt\langle\mathbf{J}^\dagger(\mathbf{r},t)\mathbf{J}^\dagger(\mathbf{r}')\rangle, \tag{1.5}$$

leads to a space-dependent, nonlocal, diffusion coefficient generalizing Eq. (1.3). In this last equation, $\mathbf{J}^\dagger$ is the dissipative (random) part of the diffusion current defined by a projection operator [13,14].

In all the approaches just mentioned, one still needs to make contact with what is measured experimentally; e.g., the net flux j of material passing through the channeled material. In steady state, this typically obeys the macroscopic phenomenological constitutive relation

$$j=P(\mu^+-\mu^-)_{z=0}, \tag{1.6}$$

where P is the permeability and $\mu^\pm$ are the chemical potentials in the $\pm$ phases. The net flow is assumed to lie along the z axis and $z=0$ is the midplane inside the channeled structure.

The simple diffusive or hopping models easily yield expressions for the permeability. The calculation based on the generalized diffusion equation, Eq. (1.4), is more involved, was considered in Ref. [15], and will be used here. Note that this theory does not assume *a priori* any reaction coordinate that dominates the dynamics of the guest.

Previous molecular dynamics simulations were performed using rigid [7–9] or flexible [10–12,16] lattices. The motion of the lattice in Refs. [10–12,16] is, again, simulated with molecular dynamics (in practice, however, the systems studied are fairly small, namely, a single unit cell containing 622 lattice atoms). In this work, the motion of the lattice is described by a generalized Langevin equation (GLE) that mimics the effect of the infinite crystal. This approach is taken for many reasons. First, with the GLE, it is possible to reproduce the vibrational density of states of the infinite crystal with high accuracy. Second, the presence of the guest will inject energy in the crystal lattice. The use of GLE allows the dissipation of that energy in a physically consistent way. In conventional MD, this extra kinetic energy would stay in the system and could later on affect the guest dynamics. As was pointed out by Kopelevich and Chang [17], there are also more subtle problems associated with classical lattice models with periodic boundary conditions; specifically, artificial feed-back mechanisms can lead to highly exaggerated sorbate transport rates in MD simulations.

Of course, for the same number of degrees of freedom, the GLE is more numerically expansive than conventional MD. If the vibrational spectrum of the infinite crystal is to be reproduced in MD simulations for typical zeolites, the motion of about 10^4 atoms needs to be simulated. Therefore, the flexibility of the lattice is often neglected in such problems. As shown by Kopelevich and Chang [17], neglecting the flexibility of the lattice does not lead to large errors for small guest in large channel structures. However, as expected, including flexibility is mandatory for a system where the size of the guest is larger than or comparable to the pore size or if the guest has to pass through small bottlenecks. In other words, one needs to include the flexibility if it changes significantly the guest available volume inside the crystal.

The importance of our approach lies in its generality. It has been shown that the use of Eqs. (1.1)–(1.3) is inconsistent for inhomogeneous systems [18]. We will show here that the transition state theory approach is not valid for systems with low energy barriers (in agreement with the prediction made in Ref. [17]) where the flexibility of the lattice can usually be neglected. When the energy barriers are large, transition state theory is expected to give a more accurate result, but in that case, the flexibility of the lattice usually plays an important role. The method proposed here is general since it includes the flexibility of the lattice self-consistently through a GLE and its applicability is independent of the magnitude of the energy barriers.

The paper is divided as follows. In Sec. II, a summary of the theory leading to a projection-operator, correlation-function expression for the macroscopic permeability is presented and we show how to approximately reexpress time correlation functions containing projected dynamics in terms of those associated with Newtonian equations of motion. The evaluation of the permeability requires a space-dependent Onsager diffusion coefficient which is obtained in terms of equilibrium time correlation functions that are computed by simulating generalized Langevin equations of motion for the guest and harmonic lattice atoms presented in Sec. II, an approach first discussed by Deutch and Silbey [19].

In Sec. III, we show how the memory functions and random noise terms that appear in the Langevin equations of motion for the crystal atoms can be calculated and we demonstrate that the vibrational density of states of the full Theta-1 crystal is reproduced. We also give an approximate way of calculating the potential of mean force for the guest inside the crystal and test it against the numerical simulations.

Section IV presents the details of the molecular model and gives results for the correlation functions and finally for the permeability for xenon in Theta-1. A detailed comparison with transition state theory is made in Sec. V. We summarize and make some concluding remarks in Sec. VI.

II. THEORY

A. Microscopic expressions for the permeability

The diffusion of the guest component inside the channeled structure is governed by the generalized diffusion equation, Eq. (1.4). The system will have many potential barriers and a nontrivial energy landscape. Microscopic expressions for the permeability starting from the generalized diffusion equation for such systems were obtained by Ronis and Vertenstein [15]. Here, we simply state their result. The macroscopic permeability of the channeled material is given by

$$\frac{1}{P}=\frac{1}{\beta}\int_{-\infty}^{+\infty}dz\left[\frac{1}{D(z)}-\frac{1}{D^{+}\Theta(z)+D^{-}\Theta(-z)}\right], \quad (2.1)$$

where,

$$D(z)\equiv\frac{1}{A}\int_{0}^{\infty}dt\int d\mathbf{r}_{\parallel}\int d\mathbf{r}'\langle \mathbf{J}_{z}^{\dagger}(\mathbf{r},t)\mathbf{J}_{z}^{\dagger}(\mathbf{r}')\rangle. \quad (2.2)$$

In these last equations, $D(z)$ is a space-dependent Onsager diffusion coefficient, $D_{\pm}$ is the bulk chemical potential in the $\pm$ phases, $\mathbf{J}_{z}^{\dagger}$ is the z component of the irreversible part of the current, and A is the area of the crystalline medium. The integral over $r_{\parallel}$ (x,y) is a consequence of the fact that the net current through the interface is along the z axis. Note that this result is first order in membrane excess quantity and this choice of $D(z)$ makes the higher order corrections smaller.

The expression for the permeability, Eq. (2.1), was derived on the basis of Eq. (1.6). The chemical potentials appearing in Eq. (1.6) are the bulk chemical potentials of the two regions extrapolated to the $z=0$ plane. It is more convenient to rewrite Eq. (1.6) in terms of the chemical potential at the two outer surfaces of the channeled medium. Since j is constant in the bulk in steady states, we rewrite Eq. (1.6) as

$$j=P'[\mu(d)-\mu(-d)], \quad (2.3)$$

where $2d$ is the thickness of the interface and

$$\frac{1}{P'} = \frac{1}{\beta}\int_{-d}^{d} dz \frac{1}{D(z)} \tag{2.4}$$

is a permeability intrinsic to the material.

B. Correlation function expression for $D(z)$

We already have a correlation function expression for the space-dependent Onsager diffusion coefficient $D(z)$ in Eq. (2.2). Unfortunately, this equation cannot be used directly to compute $D(z)$ because it involves the random part of the current. A common practice is to set $\mathbf{J}^{\dagger}=\mathbf{J}$, but, as was shown in Ref. [18], this is only valid in special cases, and in general, it is not valid in systems that are spatially inhomogeneous. A correlation function expression for $D(z)$ that approximately includes the effects of the projection operator on the time dependence of the memory function was obtained by Ronis and Vertenstein [15] in terms of unprojected time correlation functions. Their final expression for $D(z)$ is

$$D(z) = \frac{n_{\infty}\int_0^{\infty} dt \langle v_{G,z}(t) v_{G,z}\rangle_z e^{-\beta W(z)}}{1+\int_0^{\infty} dt \langle \beta F(z(t)) v_{G,z}\rangle_z}, \tag{2.5}$$

where n_{∞} is the number density in the bulk, $v_{G,z}$ is the z component of the guest velocity, $W(z)$ and $F(z)$ are, respectively, the plane average potential of mean force and the mean force. Also, $\langle\cdots\rangle_z$ denotes an equilibrium conditional average for trajectories whose initial z coordinate is z. Infinite dilution was also assumed deriving Eq. (2.5). The correlations that appear in this expression will be evaluated by the means of numerical simulations of the particle dynamics below. Given the correlation functions that appear on the right-hand side of Eq. (2.5), the calculation of the permeability is trivial. The equations of motion that will be used in the numerical simulations are described next.

C. Equations of motion

In this section, the equations of motion for the diffusing particle (hereafter referred to as the ''guest'') and the rest of the silicate atoms are described. For practical purposes, the motion of a relatively small number of crystal atoms must be simulated. The atoms in this part of the channel will be referred to as the target atoms and the rest of the crystal is called the bath. One of the main goals of this work is to preserve the effects of the crystalline bath on the motion of the target and guest atoms. In order to do this, we will use a projection operator approach introduced by Deutch and Silbey [19] in their derivation of the Langevin equation of motion for a particle in a harmonic lattice. This approach was subsequently used by Tully in his work on gas-surface interactions [20] and by Adelman, Diebold, and Mou [21] in their work on gas-solid energy exchange processes.

By assuming that the guest does not directly interact with the bath and that the crystal is fully harmonic, the equations of motion of the reduced (guest and target) system are

$$\frac{d\mathbf{p}_G(t)}{dt} = -\frac{\partial U(\mathbf{r}_G, \mathbf{r}_{\alpha_1}, \ldots, \mathbf{r}_{\alpha_{N_{\text{Target}}}})}{\partial \mathbf{r}_G} \tag{2.6}$$

and

$$\frac{d\mathbf{p}_{\alpha}}{dt} = -\frac{\partial U(\mathbf{r}_G, \mathbf{r}_{\alpha_1}, \ldots, \mathbf{r}_{\alpha_{N_{\text{Target}}}})}{\partial \mathbf{r}_{\alpha}} + e^{iLt}\langle \mathbf{F}_{\alpha}\rangle_{\text{Bath}} + \mathbf{F}_{\alpha}^{\dagger}(t) - \int_0^t dt_1 \sum_{\gamma=1}^{N_{\text{Target}}} \frac{\langle \mathbf{F}_{\alpha}^{\dagger}(t-t_1)\mathbf{F}_{\gamma}^{\dagger}\rangle_{\text{Bath}}}{m_{\gamma}k_B T}\cdot \mathbf{p}_{\gamma}(t_1), \tag{2.7}$$

where

$$\mathbf{F}_{\alpha}^{\dagger}(t) \equiv e^{iL_{\text{Bath}}t}(1-P)\mathbf{F}_{\alpha} \tag{2.8}$$

is the contribution to the force on the αth target atom at time t exerted by the bath in the presence of the *frozen* target atoms. In the last equations, the classical Liouville operator ($iL = iL_{\text{Target}} + iL_{\text{Bath}}$) has been introduced in addition to another projection operator. The projection operator $\langle\cdots\rangle_{\text{Bath}}$ is a normalized average over the bath degrees of freedom.

Note, that the projection operator no longer appears in the time dependence of $F^{\dagger}(t)$, and moreover, as was shown in Ref. [19], will evolve independently of the guest-target motion; as such, Eq. (2.7) is a generalized Langevin equation. $\mathbf{F}_{\alpha}^{\dagger}(t)$ is a colored noise and is considered in more detail in the next section. The last term on the right hand side of Eq. (2.7) is the expected friction term where the memory comes in through a force-force time correlation function.

Note that it is possible to further project out the equations of motion for the target atoms if we linearize the guest-target interaction with respect to the target coordinates. This is basically the assumption of Deutch and Silbey, cf. Ref. [19], and this approach was taken by Kopelevich and Chang [17]. This approximation is not valid when the size of the guest is comparable to or smaller than the pore sizes. Finally, note that the assumption that the guest does not interact directly with the bath can be relaxed if we can linearize the guest-bath forces in the bath degrees of freedom; this modifies Eq. (2.7) slightly, and in particular, makes the memory function depend on the instantaneous position of the guest at time t_1. In the next section, we show how the force-force correlation function can be calculated, and put everything together in order to perform the simulations.

III. IMPLEMENTATION

A. Effective forces and force correlation functions

In this section, we reexamine Eq. (2.7) and show how the various terms that appear can be calculated. The separation of crystal atoms into target and bath subspaces allows us to block the force constant matrix K as follows

$$\mathsf{K} = \begin{pmatrix} \mathsf{K}_{TT} & \mathsf{K}_{TB} \\ \mathsf{K}_{BT} & \mathsf{K}_{BB} \end{pmatrix}, \tag{3.1}$$

where K_{TT} is the $3N_{\text{Target}}\times 3N_{\text{Target}}$ matrix linking atoms in the target subspace and K_{BB} is a $3N_{\text{Bath}}\times 3N_{\text{Bath}}$ matrix linking atoms in the bath subspace only. The two rectangular matrices K_{BT} and K_{TB} connect the bath and target atoms. The first term of Eq. (2.7) can be written in matrix notation as

$$e^{iLt}\langle \mathsf{F}_T\rangle_{\text{Bath}} = e^{iLt}\langle -\mathsf{K}_{TT}\mathsf{r}_T - \mathsf{K}_{TB}\mathsf{r}_B\rangle_{\text{Bath}}, \tag{3.2}$$

where F_T, r_T, and r_B are, respectively, $3N_{\text{Target}}$, $3N_{\text{Target}}$, and $3N_{\text{Bath}}$ column vectors. The Gaussian averages are performed to give

$$e^{iLt}\langle \mathsf{F}_T\rangle_{\text{Bath}} = -\mathsf{K}_{\text{eff}}\mathsf{r}_T(t), \tag{3.3}$$

where

$$\mathsf{K}_{\text{eff}} \equiv \mathsf{K}_{TT} - \mathsf{K}_{TB}\mathsf{K}_{BB}^{-1}\mathsf{K}_{BT} \tag{3.4}$$

is an effective force constant matrix governing the harmonic motion of the target atoms in the presence of the bath.

We now derive an expression for the force correlation function. Recall that $\mathsf{F}_T^{\dagger}(t)$ is the force on the target exerted by the bath when the target atoms are frozen. In that case, the dynamics of the bath atoms are governed by

$$\mathsf{M}_B\frac{d^2\mathsf{r}_B'(t)}{dt^2} = -\mathsf{K}_{BB}\mathsf{r}_B'(t), \tag{3.5}$$

where

$$\mathsf{r}_B'(t) \equiv \mathsf{r}_B(t) + \mathsf{K}_{BB}^{-1}\mathsf{K}_{BT}\mathsf{r}_T. \tag{3.6}$$

In the last equations, M_B is the diagonal matrix containing the masses of the bath atoms.

The $3N_{\text{Bath}}$ eigenvectors $\mathsf{u}_{B,i}$ of the matrix K_{BB} are determined by

$$\tilde{\mathsf{K}}_{BB}\mathsf{u}_{B,i} = \omega_i^2\mathsf{u}_{B,i}, \tag{3.7}$$

where

$$\tilde{\mathsf{K}}_{XY} \equiv \mathsf{M}_X^{-1/2}\mathsf{K}_{XY}\mathsf{M}_Y^{-1/2} \quad \text{with } X,Y = T \text{ or } B, \tag{3.8}$$

and where ω_i^2 is the eigenvalue associated with the ith eigenvector. The shifted displacement vector $\mathsf{r}_B'(t)$ can be expanded in terms of the mass scaled eigenvectors $\tilde{\mathsf{u}}_{B,i} = \mathsf{M}_B^{-1/2}\mathsf{u}_{B,i}$ as

$$\mathsf{r}_B'(t) = \sum_{i=1}^{3N_{\text{Bath}}} \tilde{\mathsf{u}}_{B,i}\left(a_i\cos(\omega_i t) + \frac{b_i}{\omega_i}\sin(\omega_i t)\right), \tag{3.9}$$

where the a_i and b_i are related to initial positions and velocities, respectively, of the bath atoms and are Gaussian distributed. The random force, Eq. (2.8), is

$$\mathsf{F}_T^{\dagger}(t) = -\mathsf{K}_{TB}\mathsf{r}_B'(t), \tag{3.10}$$

in matrix notation, and this can be rewritten in terms of the mass-scaled eigenvectors as

$$\mathsf{F}_T^{\dagger}(t) = -\mathsf{K}_{TB}\sum_{i=1}^{3N_{\text{Bath}}} \mathsf{u}_{B,i}'\left(a_i\cos(\omega_i t) + \frac{b_i}{\omega_i}\sin(\omega_i t)\right). \tag{3.11}$$

Since the a_i and b_i in the last equation are Gaussian distributed, Eq. (3.11) shows that $\mathsf{F}_T^{\dagger}(t)$ is a Gaussian colored noise. Moreover, the random force-force correlation function is given by $\langle \mathsf{F}_T^{\dagger}(t)(\mathsf{F}_T^{\dagger})^T\rangle_{\text{Bath}}$, and from Eq. (3.11), is easily written as

$$\langle \mathsf{F}_T^{\dagger}(t)(\mathsf{F}_T^{\dagger})^T\rangle_{\text{Bath}} = k_B T\mathsf{K}_{TB}\mathsf{M}_B^{-1/2} \times \sum_{i=1}^{3N_{\text{Bath}}} \mathsf{u}_{B,i}\mathsf{u}_{B,i}^T\frac{\cos(\omega_i t)}{\omega_i^2}\mathsf{M}_B^{-1/2}\mathsf{K}_{BT}, \tag{3.12}$$

where we have expressed the $\mathsf{u}_{B,i}'$ in terms of the original eigenvectors $\mathsf{u}_{B,i}$, and where $\langle a_i^2\rangle = k_B T/\omega_i^2$.

As it turns out, the vibrational density of states of the infinite crystal is reproduced when the bath contains $O(10^4)$ atoms. Therefore, Eq. (3.12) is not particularly convenient. In other words, the required eigenanalysis may be numerically too demanding.

1. Brute force

The last section gives us a way of calculating the force-force correlation function in the time domain. By performing a Laplace transform on Eq. (3.12) and using the fact that

$$\sum_i \mathsf{u}_{B,i}\omega_i^2\mathsf{u}_{B,i}^T = \tilde{\mathsf{K}}_{BB}, \tag{3.13}$$

we obtain,

$$\langle \mathsf{F}_T^{\dagger}(s)(\mathsf{F}_T^{\dagger})^T\rangle = \frac{1}{\beta}\mathsf{M}_T^{1/2}\tilde{\mathsf{K}}_{TB}\frac{s}{\tilde{\mathsf{K}}_{BB}(s^2 + \tilde{\mathsf{K}}_{BB})}\tilde{\mathsf{K}}_{BT}\mathsf{M}_T^{1/2}, \tag{3.14}$$

where s is the Laplace transform variable. This last form of the force-force correlation function does not require an eigenanalysis. Instead, it requires the inversion of a large matrix. Inversion of matrices requires less numerical effort than a full eigenanalysis, especially when the matrices involved are sparse. Also, the Laplace representation will be more convenient to use in the simulations.

The inversion of a matrix of rank N requires $O(N^2)$ computer memory and a simple estimate shows that our computation cannot be done on most common computers. One way out of this problem is to make an approximation about the nature of the forces within the crystal. From now on, we assume that the crystal atoms interact with their nearest neighbors through stretching interactions and with their second nearest neighbors through bending interactions, and that these are the only interactions present. Hence, the force constant matrix will be massively sparse and this allows us to perform the inversion in Eq. (3.14) even if K_{BB} is large. This approach approximates the effect of the infinite bath using a

large, but finite part of the crystal that reproduces the vibrational density of state accurately. We refer to this approach as the ''brute force'' method.

2. Brillouin zones and defects

In this section, we will demonstrate how the force-force correlation function can be calculated in an exact way. This approach uses ideas first introduced by Maradudin in his study of defects in solids [22]. We rewrite Eq. (3.14) as

$$\langle \mathsf{F}_T^\dagger(s)(\mathsf{F}_T^\dagger)^T\rangle = [\Lambda(0)-\Lambda(s)]/s, \tag{3.15}$$

where

$$\Lambda(s) \equiv \beta^{-1}\mathsf{M}_T^{1/2}\tilde{\mathsf{K}}_{TB}\mathsf{G}(s)\tilde{\mathsf{K}}_{BT}\mathsf{M}_T^{1/2}, \tag{3.16}$$

with

$$\mathsf{G}(s) \equiv [s^2+\tilde{\mathsf{K}}_{BB}]^{-1}. \tag{3.17}$$

As before, the problem with the last expression lies in the inversion of a large matrix. The function $\mathsf{G}_0(s)$ defined as $\mathsf{G}_0(s)\equiv[s^2+\tilde{\mathsf{K}}]^{-1}$, where $\tilde{\mathsf{K}}$ is the mass-scaled force constant matrix for the full crystal, can be obtained exactly by using a Fourier representation and then integrating over the first Brillouin zone of the crystal. We assume that $\mathsf{G}_0(s)$ is known and obtain $\Lambda(s)$ in terms of it. To proceed, we reblock $\tilde{\mathsf{K}}$ in the following way:

$$\tilde{\mathsf{K}} = \begin{pmatrix} \tilde{\mathsf{K}}_{TT} & \tilde{\mathsf{K}}_{TB_1} & \tilde{\mathsf{K}}_{TB_2} \\ \tilde{\mathsf{K}}_{B_1T} & \tilde{\mathsf{K}}_{B_1B_1} & \tilde{\mathsf{K}}_{B_1B_2} \\ \tilde{\mathsf{K}}_{B_2T} & \tilde{\mathsf{K}}_{B_2B_1} & \tilde{\mathsf{K}}_{B_2B_2} \end{pmatrix}, \tag{3.18}$$

where we have split the bath into two parts: the primary bath subspace B_1 refers to bath atoms that couple directly to the target (i.e., they have a target atom as their nearest or second nearest neighbor); the secondary bath subspace B_2 contains atoms that are not directly coupled with the target atoms (clearly, B_2 is much larger than the other subspaces). Note that $\tilde{\mathsf{K}}_{TB_2}=\tilde{\mathsf{K}}_{B_2T}=0$.

We write $\tilde{\mathsf{K}}_{BB}=\tilde{\mathsf{K}}-\tilde{\Delta}$, where

$$\tilde{\Delta} \equiv \begin{pmatrix} \tilde{\mathsf{K}}_{TT} & \tilde{\mathsf{K}}_{TB_1} & 0 \\ \tilde{\mathsf{K}}_{B_1T} & 0 & 0 \\ 0 & 0 & 0 \end{pmatrix},$$

and rewrite $\mathsf{G}(s)$ as

$$\mathsf{G}(s) = [s^2+\tilde{\mathsf{K}}-\tilde{\Delta}]^{-1} = [1-\mathsf{G}_0(s)\tilde{\Delta}]^{-1}\mathsf{G}_0(s). \tag{3.19}$$

We separate $\mathsf{G}_0(s)$ into blocks as

$$\mathsf{G}_0(s) = \begin{pmatrix} \mathsf{g}_{11} & \mathsf{g}_{12} \\ \mathsf{g}_{21} & \mathsf{g}_{22} \end{pmatrix}, \tag{3.20}$$

where the 1 subspace contains the target and the bath primary zone and 2 refers to the bath secondary atoms. In this representation,

$$\tilde{\Delta} \equiv \begin{pmatrix} \delta\tilde{\mathsf{K}} & 0 \\ 0 & 0 \end{pmatrix}, \tag{3.21}$$

where

$$\delta\tilde{\mathsf{K}} \equiv \begin{pmatrix} \tilde{\mathsf{K}}_{TT} & \tilde{\mathsf{K}}_{TB_1} \\ \tilde{\mathsf{K}}_{B_1T} & 0 \end{pmatrix}. \tag{3.22}$$

By evaluating $[1-\mathsf{G}_0(s)\tilde{\Delta}]^{-1}\mathsf{G}_0(s)$, we find that

$$\mathsf{G}(s) = \begin{pmatrix} (1-\mathsf{g}_{11}\delta\tilde{\mathsf{K}})^{-1}\mathsf{g}_{11} & (1-\mathsf{g}_{11}\delta\tilde{\mathsf{K}})^{-1}\mathsf{g}_{12} \\ \mathsf{g}_{21}\delta\tilde{\mathsf{K}}(1-\mathsf{g}_{11}\delta\tilde{\mathsf{K}})^{-1}\mathsf{g}_{11}+\mathsf{g}_{21} & \mathsf{g}_{21}\delta\tilde{\mathsf{K}}(1-\mathsf{g}_{11}\delta\tilde{\mathsf{K}})^{-1}\mathsf{g}_{12}+\mathsf{g}_{22} \end{pmatrix}. \tag{3.23}$$

There are still multiplications of large matrices in the last expression, but notice that the only inverse that we need, $(1+\mathsf{g}_{11}\delta\tilde{\mathsf{K}})^{-1}$, contains matrices in the 11 space. These matrices are relatively small and the inversion is much more manageable. Moreover, by noting that $\tilde{\mathsf{K}}_{TB}$ and $\tilde{\mathsf{K}}_{BT}$ are nonzero only in the 11 subspace, only the 11 block of $\mathsf{G}(s)$ is needed in order to compute $\Lambda(s)$, which thus becomes

$$\Lambda(s) = \frac{1}{\beta}\mathsf{M}_T^{1/2}\tilde{\mathsf{K}}_{TB}\frac{1}{\mathsf{g}_{11}^{-1}(s)-\delta\tilde{\mathsf{K}}}\tilde{\mathsf{K}}_{BT}\mathsf{M}_T^{1/2}, \tag{3.24}$$

using Eqs. (3.16) and (3.23). This expression is more convenient than Eq. (3.14) because it involves small matrices. Everything that we have done in this subsection is exact. It is

very simple to work with Eq. (3.24) provided that we have calculated $g_{11}(s)$ beforehand.

The periodicity of the lattice can be used to obtain $\mathsf{G}_0(s)$, and hence, $g_{11}(s)$, in terms of integrations over the Brillouin zone. Since these methods are standard (see, e.g., Ref. [23]), we simply state the result; i.e.,

$$[\mathsf{G}_0(s)]_{i,j}^{\alpha,\beta}=\left[\frac{1}{s^2+\tilde{\mathsf{K}}}\right]_{i,j}^{\alpha,\beta}=\int' \frac{d\mathbf{k}}{(2\pi)^3}e^{i\mathbf{k}\cdot(\mathbf{R}_i-\mathbf{R}_j)}\sum_p \frac{\epsilon_p^\alpha(\mathbf{k})[\epsilon_p^\beta(\mathbf{k})]^T}{s^2+\omega_p^2(\mathbf{k})}, \tag{3.25}$$

where the indices i and j indicate which unit cell the atoms lie in, and where α and β denote the atoms within the unit cell and the Cartesian components of the displacements. The prime on the integral sign restricts the integration to the first Brillouin zone of the crystal. Also, $\omega_p^2(\mathbf{k})$ and $\epsilon_p(\mathbf{k})$ are, respectively, the pth eigenvalues and eigenvectors of the matrix $\tilde{\mathsf{K}}(\mathbf{k})$ defined by

$$\tilde{\mathsf{K}}^{\alpha,\beta}(\mathbf{k})\equiv\sum_{\mathbf{R}} e^{-i\mathbf{k}\cdot\mathbf{R}}\tilde{\mathsf{K}}_{\mathbf{R}}^{\alpha,\beta}, \tag{3.26}$$

where $\mathbf{R}$ is the lattice vector connecting the respective unit cells of atoms α and β.

This method requires an eigenanalysis of a matrix of rank $3N_0$, for every wave number $(\mathbf{k})$, where N_0 is the number of atoms in the unit cell. On the other hand, the numerical evaluation of the Fourier transform has to be done carefully such that an accurate result is obtained. In particular, the sampling of wave vectors has to be on a scale finer than $2\pi/|\mathbf{R}_i-\mathbf{R}_j|$, which is a problem when large separations are needed.

Thus, we have two ways of calculating the force-force correlation function. The first, is a brute force way in the sense that we make the bath as large as we can (the upper bound is determined by the amount of computer memory we can use) and perform the matrix inversion using a sparse subroutine. The other approach is to use the theory of defects together with a Brillouin zone calculation of $\mathsf{G}_0(s)$. This approach is exact on paper, but the numerical integration prescribed by Eq. (3.25) introduces inaccuracies. Another approach would be to approximate the $\mathbf{k}$ dependence of $\omega_p(\mathbf{k})$ and do the integrals exactly. We tried all three approaches and they give comparable results. We decided to use the brute force method as it is free of the above problem.

B. Differential equations

The Langevin equation derived in Sec. II C is not convenient for numerical use. First, while we are able to calculate the force-force correlation function in time or frequency, we do not have a simple analytic representation for this function. All we have are inefficient ways to obtain the function at a discrete collection of points. Second, the Langevin equation is a stochastic colored-noise integro-differential equation. In this section, we drop the integral term in Eq. (2.7) at the expense of introducing extra dynamical fields, and in order to do this, we introduce an analytic approximation to the memory functions.

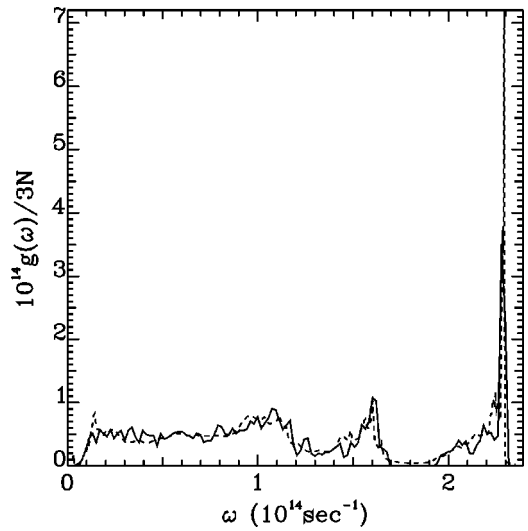

FIG. 1. The exact density of states (full line) for Theta-1 obtained in a Brillouin zone calculation is compared with the approximate density of states (dashed line) that is generated using our representation of the memory function, Eq. (3.27). The force constants are specified in Sec. IV A.

In frequency space, the force-force correlation function is described by Eq. (3.14). We approximate the Laplace transform of the memory function matrix as

$$\beta\langle\mathsf{F}_T^\dagger(s)\mathsf{F}_T^{\dagger T}\rangle\approx\frac{s}{\mathsf{A}+\mathsf{B}s+\mathsf{C}s^2}, \tag{3.27}$$

where A, B, and C are $3N_{\text{Target}}\times 3N_{\text{Target}}$ matrices. Analytical expressions for A and C can be obtained from the $s\to 0$ and $s\to\infty$ limit of Eq. (3.14). After examining several different schemes for obtaining B, each giving roughly equivalent results, we decided to obtain the A and the B matrices from a linear least square fit while the C matrix was obtained from the asymptotic relations. Note that our approximation for the memory functions captures the decay and the oscillatory behavior of the memory function.

As shown in Ref. [20], the vibrational density of states $g(\omega)$ can be expressed in terms of the memory function as

$$g(\omega)=\text{Tr}\{\text{Re}[\tilde{\mathsf{C}}(i\omega)]\}, \tag{3.28}$$

where

$$\tilde{\mathsf{C}}(s)\equiv\left(s+\frac{\tilde{\mathsf{K}}_{\text{eff}}}{s}+\beta\mathsf{M}^{-1/2}\langle\mathsf{F}_T^\dagger(s)\mathsf{F}_T^{\dagger T}\rangle\mathsf{M}^{-1/2}\right)^{-1}. \tag{3.29}$$

In Fig. 1, we compare the approximate vibrational density of states with the exact result calculated using Brillouin zone sums. The agreement is excellent.

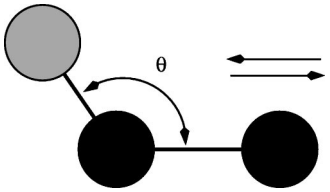

FIG. 2. In this figure, the gray atom is a bath atom while the black ones are target atoms. The motion of the second target atom is illustrated. For potentials that include only stretching and bending energies, the bath atom does not feel the motion since the angle θ remains unchanged.

Note that the matrix $\langle \mathsf{F}_T^{\dagger}(s)\mathsf{F}_T^{\dagger\,T}\rangle$ does not have a rank equal to $3N_{\text{Target}}$. This is expected since every atom in the target space does not interact directly with the bath. In fact, for the harmonic interactions considered here, only target atoms which have a bath atom as their nearest or second-nearest neighbor can interact with the bath, and only these have nonzero random forces. In reality, the rank of the matrix is even smaller (e.g., as indicated by extra zero eigenvalues). This implies that there are extra motions of the target atoms that do not couple to the bath. An example of such a motion is illustrated in Fig. 2. Therefore, henceforth, we work in a reduced space (where A, B, and C are nonsingular) determined by the number independent target motions that couple to the bath.

With our expression, Eq. (3.27), for the force-force correlation function, we can replace the noise and friction term in the Langevin equation, Eq. (2.7), by an extra dynamical field, $-\dot{\mathsf{y}}(t)$. The equations of motion for the guest and target atoms are now written as

$$\frac{d\mathbf{p}_G(t)}{dt} = -\frac{dU[\mathbf{r}_G(t),\mathsf{R}_T(t)]}{d\mathbf{r}_G}, \tag{3.30}$$

$$\frac{d\mathsf{P}_T(t)}{dt} = -\mathsf{K}_{\text{eff}}\mathsf{R}_T(t) - \frac{dU[\mathbf{r}_G(t),\mathsf{R}_T(t)]}{d\mathsf{R}_T} - \dot{\mathsf{y}}(t), \tag{3.31}$$

and

$$\left(\mathsf{C}\frac{d^2}{dt^2} + \mathsf{B}\frac{d}{dt} + \mathsf{A}\right)\mathsf{y}(t) = \boldsymbol{\eta}(t) + \mathsf{M}^{-1}\mathsf{P}_T(t). \tag{3.32}$$

The extra dynamical field $\mathsf{y}(t)$ is a generalized Ornstein-Uhlenbeck process [24] with random initial conditions that satisfy

$$\langle \mathsf{y}\mathsf{y}^T\rangle = k_B T\mathsf{A}^{-1}, \tag{3.33a}$$

$$\langle \dot{\mathsf{y}}\mathsf{y}^T\rangle = \langle \mathsf{y}\dot{\mathsf{y}}^T\rangle = 0, \tag{3.33b}$$

and

$$\langle \dot{\mathsf{y}}\dot{\mathsf{y}}^T\rangle = k_B T\mathsf{C}^{-1}, \tag{3.33c}$$

and where the white noise variable $\boldsymbol{\eta}(t)$ satisfies

$$\langle \boldsymbol{\eta}(t)\,\boldsymbol{\eta}(t')^T\rangle = k_B T\mathsf{B}\delta(t-t'). \tag{3.33d}$$

In Appendix A we show that this set of equations of motion for the target atoms is equivalent to Eq. (2.7), as long as the memory function can be written as in Eq. (3.27).

C. Potential of mean force approximation

At this point, we have everything that we need to perform simulations of the guest motion inside the channel used to calculate the correlation functions appearing in the diffusion coefficient [cf. Eq. (2.5)]. The only quantity that is still missing is the plane potential of mean force. In this section, we derive an approximation for the potential of mean force $W(\mathbf{r}_G)$ for the guest in the channeled structure.

The mean force, $\mathbf{F}(\mathbf{r}_G)$, can be obtained from the following potential of mean force:

$$\begin{aligned} W(\mathbf{r}_G) &= -k_B T \ln\left[\int d\mathsf{R}_T e^{-\beta[1/2\mathsf{R}_T^T\mathsf{K}_{\text{eff}}\mathsf{R}_T + U(\mathbf{r}_G,\mathsf{R}_T)]}\right] \\ &= -k_B T \ln\left[\int d\mathsf{R}_T e^{-\beta U'}\right], \end{aligned} \tag{3.34}$$

where the definition of U' is obvious and where R_T is now the displacement of the target atoms from their equilibrium positions in the absence of the guest. The interaction potential between the target and the guest, which is still unspecified, will not have a simple linear or quadratic form. Therefore, in general, the integral appearing in the last equation cannot be done analytically. Nonetheless, given the stiffness of the lattice, we can find a good approximation for $W(\mathbf{r}_G)$.

We rewrite the target displacement vector as $\mathsf{R}_T = \mathsf{R}_T^{(0)} + \delta\mathsf{R}_T$ and Taylor expand the interaction potential about $\mathsf{R}_T^{(0)}$. For the following choice for $\mathsf{R}_T^{(0)}$,

$$\mathsf{K}_{\text{eff}}\mathsf{R}_T^{(0)} = \mathsf{F}(\mathbf{r}_G,\mathsf{R}_T^{(0)}); \tag{3.35}$$

i.e., the position where the net force on the target atoms vanishes, the potential of mean force can be rewritten as

$$\begin{aligned} W(\mathbf{r}_G) = U(\mathbf{r}_G,\mathsf{R}_T^{(0)}) &+ \frac{1}{2}\mathsf{R}_T^{(0)T}\mathsf{K}_{\text{eff}}\mathsf{R}_T^{(0)} \\ &- k_B T \ln\left(\int d\,\delta\mathsf{R}_T e^{-\beta/2\delta\mathsf{R}_T^T\mathsf{D}(\mathbf{r}_G)\delta\mathsf{R}_T}\right) \\ &- k_B T \ln\langle e^{-\beta\delta U}\rangle, \end{aligned} \tag{3.36}$$

where

$$\mathsf{D}(\mathbf{r}_G) \equiv \mathsf{K}_{\text{eff}} + \frac{\partial^2 U(\mathbf{r}_G,\mathsf{R}_T^{(0)})}{\partial\mathsf{R}_T^2}, \tag{3.37}$$

$$\langle(\cdots)\rangle = \frac{\int d\,\delta\mathsf{R}_T e^{-\beta/2\delta\mathsf{R}_T^T\mathsf{D}(\mathbf{r}_G)\delta\mathsf{R}_T}(\cdots)}{\int d\,\delta\mathsf{R}_T e^{-\beta/2\delta\mathsf{R}_T^T\mathsf{D}(\mathbf{r}_G)\delta\mathsf{R}_T}}, \tag{3.38}$$

and

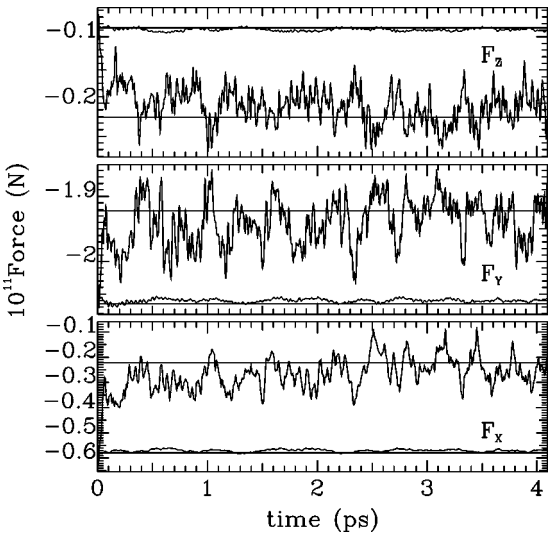

FIG. 3. The force acting on xenon in Theta-1 during the aging is shown as the noisy curves. The curve showing large fluctuations is obtained at 300 K, the other at 3 K. The straight lines are the approximate values for the mean force at 300 K and 3 K. The guest is at (6.49633 Å, 8.07333 Å, 2.36156 Å). The system and the potential are defined in Sec. IV A

$$\delta U = \frac{1}{3!}\frac{\partial^3 U(\mathbf{r}_G, \mathsf{R}_T^{(0)})}{\partial \mathsf{R}_T^3} \times \mathsf{R}_T^3 + \cdots, \tag{3.39}$$

where the $\times$ in the last equation implies that the multidimensional matrix product is taken appropriately. The first integral is just another Gaussian integral while the $\ln\langle e^{-\beta\delta U}\rangle$ can be expanded in cumulants (see Ref. [25]). By neglecting terms that do not contribute to the mean force, we can write the full expression for the potential of mean force as

$$W(\mathbf{r}_G) = U(\mathbf{r}_G, \mathsf{R}_T^{(0)}) + \frac{1}{2}\mathsf{R}_T^{(0)T}\mathsf{K}_{\text{eff}}\mathsf{R}_T^{(0)} + \frac{k_B T}{2}\ln\{\det[\mathsf{K}_{\text{eff}}^{-1}\mathsf{D}(\mathbf{r}_G)]\} - k_B T\sum_{j=1}^{\infty}\frac{\langle\langle(-\beta\delta U)^j\rangle\rangle}{j!}, \tag{3.40}$$

where $\langle\langle\cdots\rangle\rangle$ are cumulant averages and where the potential has been shifted by constants so as to vanish when the guest is noninteracting.

At low temperatures, the first temperature correction to the potential of mean force will be linear in T, and the cumulants give higher order temperature corrections. In this work, we only keep the linear temperature dependence and drop the remaining terms; this turns out to give an excellent approximation at room temperature for our system. In Fig. 3, we compare the numerically simulated force on a frozen guest with that obtained from Eq. (3.40).

This section will be concluded with a brief remark. In the simulations, before releasing the guest, the lattice must be aged such that the target atoms have enough time to shift their equilibrium positions to ones that, on average, minimize the free energy of the system. Another scenario may be that, during the aging, the target atoms undergo a uniform collective translation that would put the guest at a minimum. Clearly, this should not happen. In order to prevent such a collective motion, we tethered some of the edge atoms of the bath (specifically, those atoms that were not fully coordinated). In Appendix B, by using continuum elastic theory, we show that the tethering of boundary atoms does what we want for a three-dimensional system, namely, it makes a uniform translation of the target atoms impossible without an energy cost. On the other hand, this simple calculation shows that for one- and two-dimensional systems, the translation of a small portion inside the crystal costs no energy even though the edges of the crystal are tethered, and is another manifestation of the well known Mermin-Wagner instability in low dimensional solids [26].

IV. RESULTS

A. Specification of the system and potentials

In this section, we briefly describe the system that we will be working with. In particular, we specify the harmonic force constants and the form of the guest-target interaction potential. For practical purposes, we chose a sodalite having disconnected, one-dimensional, channels. This will allow us to calculate plane averages using a single channel. The zeolite we chose is Theta-1 (TON). This system is a high silicate zeolite. We therefore assume that it has no Al atoms and thus, has the further advantage of not having any counter ions. Theta-1 contains two ten-membered oxygen-ring channels per unit cell. The target space that we used contains five unit cells along z and embeds the channel out to a radius of 6.5 Å from the channel axis. The target zone contains 210 atoms (140 oxygens and 70 silicons) and is electrically neutral. The crystallographic unit cell for Theta-1 is cubic and is described in Ref. [27]. The full unit cell contains 72 atoms. Notice that there is a reflection plane in x through the middle of the unit cell. The target zone is depicted in Fig. 4. The harmonic force constants were obtained from Ref. [28] and are summarized in Table I.

We assume that the potential energy of xenon inside a sodalite is well described by a Lennard-Jones term plus an induced dipole-electric field interaction; i.e.,

$$U(\mathbf{r}_G, \mathbf{r}_1, \ldots, \mathbf{r}_{N_{\text{Target}}}) = \sum_{i=1}^{N_{\text{Target}}} 4\epsilon_{i,G}\left[\left(\frac{\sigma_{i,G}}{r_{i,G}}\right)^{12} - \left(\frac{\sigma_{i,G}}{r_{i,G}}\right)^{6}\right] - \frac{\alpha_G}{2}\mathbf{E}\cdot\mathbf{E}, \tag{4.1}$$

where

$$\mathbf{E} \equiv \sum_{i=1}^{N_{\text{Target}}}\frac{q_i \mathbf{r}_{i,G}}{4\pi\epsilon_0 r_{i,G}^3} \tag{4.2}$$

is the electric field felt by the noble gas atom due to the partial charges on the crystal atoms. In the last two equations, $r_{i,G} \equiv |\mathbf{r}_i - \mathbf{r}_G|$, $\epsilon_{i,G}$ and $\sigma_{i,G}$ are the Lennard-Jones

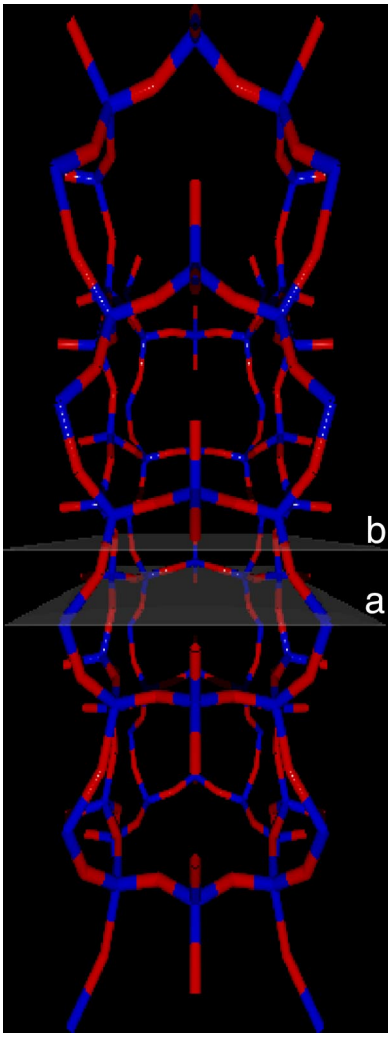

FIG. 4. (Color online) The target zone. The oxygen atoms are in red and the silicon atoms are in blue. A minimum (a) and a maximum (b) $W(z)$ plane are shown. Note that the binding pocket is on the near side of the channel for the plane (a).

parameters related to the guest-Si or guest-O interactions, ϵ_0 is the permittivity of vacuum, q_i is the partial charge on the ith target atom, and α_G is the polarizability of the guest.

There seems to be a consensus for the calculated values of the partial charges in silicates in the quantum mechanical literature (see, e.g., Refs. [29,30]); namely, $q_0=-1.2e$ and $q_{Si}=2.4e$, where e is the electron charge. For the values of the Lennard-Jones parameters, we did not find good agreement in the literature. A common way to proceed is to write the Lennard-Jones potential between molecule i and j as

TABLE I. Silicate force constants [28].

Motion	Force constant
Si-O stretch	5.0×10^{-18} J Å^{-2}
O-Si-O bend	1.35×10^{-18} J rad^{-2}
Si-O-Si bend	0.31×10^{-18} J rad^{-2}

$$\phi_{ij}=-\frac{A_{ij}}{r_{i,j}^6}+\frac{B_{ij}}{r_{i,j}^{12}}. \tag{4.3}$$

If we have a way to calculate A_{ij} and if we know the interatomic equilibrium separation $r_{i,j}^{eq}=2^{1/6}\sigma_{i,j}$, we can determine $\epsilon_{i,j}$. The equilibrium separation will be taken as the sum of the radius of the atoms involved, while A_{ij} is commonly determined by the London formula (cf. Ref. [31]),

$$A_{ij}=\frac{3}{2}\alpha_i\alpha_j\frac{E_iE_j}{E_i+E_j}, \tag{4.4}$$

or the Kirkwood-Muller formula (cf. Refs. [32,33]),

$$A_{ij}=6mc^2\alpha_i\alpha_j\left(\frac{\alpha_j}{\chi_j}+\frac{\alpha_i}{\chi_i}\right)^{-1}, \tag{4.5}$$

where α_i is the polarizability of atom i and χ_i is its magnetic susceptibility.

Table II contains a summary of what has been used in the literature to calculate the Lennard-Jones parameters. None of these studies used accurate partial charges for the silicon and the oxygen. In Refs. [5,6], a fully ionic structure is assumed. In Ref. [34], the oxygen partial charge is introduced solely to balance the charge of the counterions, while in Ref. [35], the partial charges are neglected. The atomic polarizability for the channel atoms determined in Refs. [5,6] seems reasonable. The values for the polarizabilities for the ionic and neutral atoms are $\alpha_O=0.802$, $\alpha_{O^{-2}}=3.88$, $\alpha_{Si}=5.38$ and $\alpha_{Si^{+4}}=0.0165$ Å^3 (cf. Ref. [36]). We expect values that are between these limiting cases for silicate atoms and the values reported in Refs. [5,6] are in that range. The other parameters in Refs. [5,6] are those of a fully ionic crystal (the radius, the ionization potential, and the magnetic susceptibility). On the other hand, Ref. [34] uses reasonable values for the polarizability while Ref. [35] uses the polarizability of neutral oxygen. In addition, Refs. [34,35] use the same oxygen radius which is bigger than that of O^{-2}. This radius is the van der Waals radius of oxygen given by Bondi [37].

Because of the lack of agreement in these approaches, we decided to use our own parameters using the accurate partial charges values and interpolating the needed parameters (E, α, . . .) from the CRC reference values (cf. Ref. [36]) of the neutral and ionized atoms. We will use the London formula with the polarizabilities of Refs. [5,6] and we will interpolate the ionization potentials for $Si^{+2.4}$ and $O^{-1.2}$ using data in the literature [36]; the parameters thus obtained are summarized in Table II. By using the London formula, Eq. (4.4), and the data in Tables III and II one obtains the Lennard-Jones parameters for the noble gas–zeolite atom interactions listed in Table IV.

Henceforth, we consider the case of xenon diffusing inside Theta-1. The potential of mean force inside the channel can be calculated using Eq. (3.40) and some constant potential of mean force surfaces are shown in Fig. 5. There are broad binding regions staggered on either side of the channel. The binding pockets are almost flat energetically; a closer examination shows that there are three binding sites in

TABLE II. Parameters for zeolites silicon and oxygen.

Ref.	Atom	$q(e)$	Radius (Å)	α (Å^3)	E(eV)	χ(cm^3/mol)$\times 10^6$
[5,6][a]	O	-2	1.40	1.65	13.55	12.58
	Si	$+4$	0.42	0.02	166.73	1.00
[34][b]	O	-0.15, -0.20	1.52	1.25, 1.40	N/A	10.0, 9.9
[35]	O	0	1.52	0.85	N/A	N/A
This work	O	-1.2	1.08	1.65	3.887	
	Si	$+2.4$	0.53	0.02	39.855	

[a]In these references, the values for all the parameters are determined from the fully ionized atoms except for α which is determined more accurately from refractivity experiments (cf. Ref. [5]).
[b]This comes from work on zeolites NaX and NaY. When two values are reported, it refers to the two zeolite types, respectively. The charge on the oxygens is there to neutralize the charge carried by the counterions. Also, it is assumed that the Si/Al atoms do not contribute to the potential.
[c]Here, the Si/Al atoms as well as the partial charges are neglected.

each pocket; one is exactly in the middle of the cell (in x) and the other two are symmetrically placed on either side. The barrier for motion between the central binding site and either of the ones to its side is very small, about $0.1k_BT$ at 300 K. Hence, there will not be any specific contributions to the permeability from the saddle points on these paths, and we have omitted them from the figures for the sake of clarity.

The figures show that it is easier for the xenon atom to move between binding sites on the same side of the channel (the energy barrier is lower). The reaction coordinate linking two minimum energy sites is also shown in these figures. Notice that one of these paths (path 1 in Fig. 5) links binding sites that lie on the same side of the channel. The other (path 2 in Fig. 5) bridges binding sites that are on opposite sides. It turns out that path 1 has a lower activation energy than path 2. The free energy (potential of mean force) is plotted against the z component along path 1 and path 2 in Fig. 6.

The potential of mean force, $W(\mathbf{r})$, can be used to calculate the plane potential of mean force, $W(z)$, as

$$e^{-\beta W(z)}=\frac{1}{A_{\mathrm{Cell}}}\int_{\mathrm{Unit\ cell}} dxdy e^{-\beta W(\mathbf{r})}, \tag{4.6}$$

where A_{Cell} is the area of the unit cell perpendicular to z and the integration is restricted to the unit cell (note that each unit cell contains two channels). The resulting plane potential of mean force along the channel axis is shown in Fig. 7. This figure also shows the minimum potential of mean force in each plane. The enthalpy of sorption, ΔH, of xenon in Theta-1 can be estimated from Ref. [5] as

$$\Delta H = W_{min} + \frac{k_BT}{2} + \frac{1}{2}\sum_{i=1}^{3}\hbar\omega_i, \tag{4.7}$$

where W_{min} is the minimum in the potential of mean force and where the last term is a sum over the zero point energy of vibration of the guest at the absolute minimum (this assumes that the potential of mean force near the minimum is almost harmonic). Assuming that this last term is small, we obtain a heat of sorption of $\Delta H \approx 6.4k_BT$ at 300 K. Experimental measurements for xenon absorbed in mordenite gives $\Delta H = 14.1k_BT$ [5] and for xenon absorbed in zeolite Na-Y, $\Delta H = 7.21k_BT$ [39] at 300 K. Since the sorption occurs in different system, we do not expect our number to agree. On the other hand, this confirms that our model potential does give heats of sorption that are the right order of magnitude. We did not find any experimental data for xenon absorbed in Theta-1. However, Ref. [35] calculates, using a rigid lattice and no polarization, a value for the activation energy of xenon in Theta-1, $E_{act}=1.24k_BT$ at 300 K. This number can be compared with the path's activation energies of Fig. 6 which gives $W_{act}=1.95k_BT$, $2.06k_BT$ or $2.15k_BT$ at 300 K depending on the path. Also, Kärger *et al.* [40] obtained an activation energy studying the self-diffusivity of xenon in silicalite [a three-dimensional (3D) interconnected ten-oxygen ring channel silicate] assuming that the temperature dependence of the self-diffusivity is well described by

$$D = D_o e^{-\beta E_{act}}. \tag{4.8}$$

TABLE III. Parameters for the noble gas atoms.

Atom	Radius (Å) [38]	α (Å^3) [36]	E(eV) [36]
Ne	1.560	0.3956	21.56460
Ar	1.900	1.6411	15.75962
Xe	2.224	4.0440	12.12980

TABLE IV. Lennard-Jones parameters for the gas-channel interactions ($T=300$ K).

Gas atom	$\sigma_{\mathrm{Si}\text{-}X}$ (Å)	$\epsilon_{\mathrm{Si}-X}/k_BT$	$\sigma_{\mathrm{O}\text{-}X}$ (Å)	$\epsilon_{\mathrm{O}\text{-}X}/k_BT$
Ne	1.8622	0.0385	2.3522	0.1841
Ar	2.1622	0.0512	2.6522	0.3440
Xe	2.4537	0.0500	2.9437	0.4378

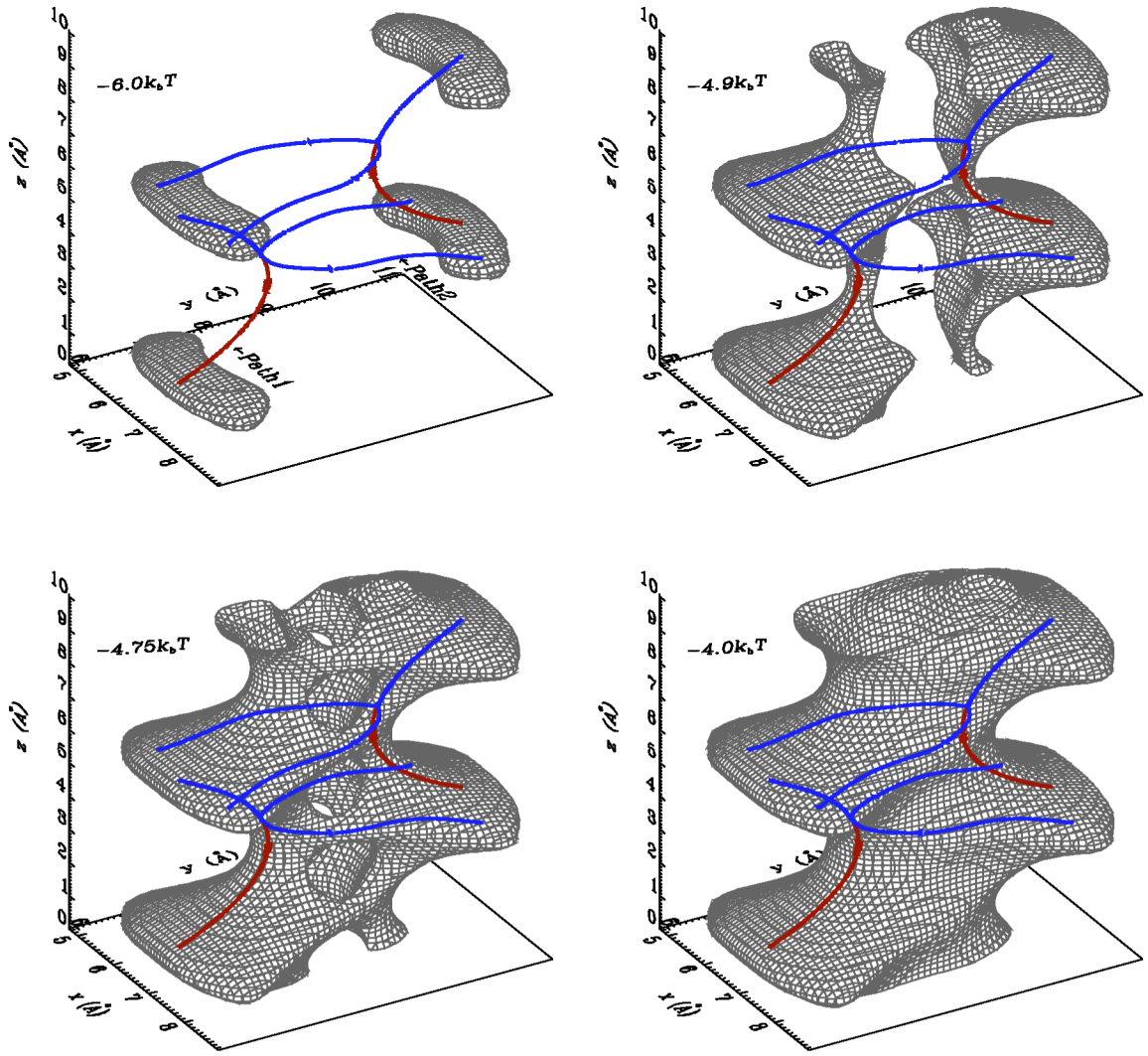

FIG. 5. (Color online) Constant potential of mean force surfaces for xenon in Theta-1 (two unit cells along the channel axis are shown) at 300 K. The surface energy is indicated in the corner of each part. The absolute minimum is at $-6.94k_BT$. Steepest descent reaction coordinates are shown in red and blue.

Their measured value was $E_{act}=2.0k_BT$ at 300 K. In our case, this should be compared with the barrier in $W(z)$ which is $1.43k_BT$. Note that in Sec. II B we assumed that the potential of mean force was defined relative to its value in the adjacent bulk phases. If an experiment is carried out where Theta-1 separates two solutions, the potential of mean force has to be shifted by the configurational Helmholtz free energy of the guest in the bulk, W_{Bulk}.

B. Simulation results and permeability of xenon in Theta-1

Before presenting the results of the simulation, there are still a few remarks that must be made. First, the simulation will have to perform many matrix-column vector multiplications. These matrices, $\mathsf{K}_{\mathrm{eff}}$, A, B, and C, are all sparse to some extent. In order to reduce the computation time, we set the elements smaller than some threshold in these matrices to zero, and then use sparse matrix routines to perform the multiplications (specifically, we used the NIST sparse subroutine package [41]). The threshold is chosen such that the effect on the vibrational density of states of the crystal is negligible. Because the induced dipole/electric field interaction in the potential is long range, we added a static bath background correction potential, obtained by the means of Ewald sums (see, e.g., Ref. [23]), in the simulations. Finally, the simulations were performed by integrating the set of differential equations, cf. Eqs. (3.30)–(3.32) using a second order stochastic Runge-Kutta integrator [42]. The aging time was 4.096×10^{-12} s and the simulation length was 8.192×10^{-12} s or 12.288×10^{-12} s. The time step used was 5.0×10^{-16} s. We calculated the correlations for every initial starting points by averaging over 2000 independent trajectories and performed this numerical work on a Beowulf cluster consisting of 16 processors.

The space dependent diffusion coefficient $D(z)/n_\infty$ is obtained from the plateau value of

$$D(z,t)=\frac{n_\infty \int_0^t dt_1 \int_{\text{Unit cell}} d\mathbf{r}_\parallel \langle v_{G,z}(t_1) v_{G,z}\rangle_{\mathbf{r}} e^{-\beta W(\mathbf{r})}}{A_{\text{Cell}}+\int_0^t dt_1 \int_{\text{Unit cell}} d\mathbf{r}_\parallel \langle \beta F(z(t_1)) v_{G,z}\rangle_{\mathbf{r}} e^{-\beta[W(\mathbf{r})-W(z)]}}, \tag{4.9}$$

where $W(\mathbf{r})$ is the potential of mean force at a point, $W(z)$ is the plane potential of mean force defined in Eq. (4.6) and A_{Cell} is the xy area of the unit cell. Each plane integration was performed using a grid that contains between 25 and 48 points, chosen in such a way that the potential of mean force in that plane and the plane average potential of mean force are accurately reproduced. The correlation functions were obtained from the numerical simulations and space group symmetries pertaining to a single channel were used to reduce the numerical effort (by four). Values between the grid points were interpolated using a bicubic spline and these were used to numerically perform the plane integration. The quantity $D(z,t)e^{\beta W(z)}/n_\infty$ is shown in Figs. 8 and 9 for $z=2.519$ [maximum $W(z)$ plane], and 0.944 625 Å [minimum $W(z)$ plane].

Figures 8 and 9 also illustrate the effect that the correction term in the denominator in Eq. (4.9) has on the integral of the velocity correlation function. In fact, neglecting that correction is equivalent to neglecting the † on the current fields **J** in Eq. (1.5) which has been shown to be incorrect [18], even if the naive Green-Kubo integral converges. Also, note that the correction factor in the maximum $W(z)$ plane lowers the average of the velocity correlation function integral (see Fig. 8), while it raises the average of the velocity correlation function integral in the minimum $W(z)$ plane. The effect of the correction in the minimum energy plane is in agreement with the prediction made in Ref. [18].

The dynamics can change the relative contributions to $D(z)$ within a given plane over what would be expected simply on the basis of the Boltzmann weight (e.g., as in a Smoluchowski approach). This is illustrated in Fig. 10. It is clear from these figures that the dynamics can drastically affect the shape of the various contributions within a given plane. Regions with low potentials often have less correlated dynamics, while those with high potentials will have more coherent motion; what contributes to $D(z)$ is a compromise between the Boltzmann weight and the coherence of the motion.

Table V lists the calculated space-dependent diffusion coefficient $D(z)/n_\infty$ for several planes. We also show these results graphically in Fig. 11 for one unit cell along z. In Sec. II A, we assumed that the quantity $D(z)e^{\beta W(z)}$ is constant near the barrier tops. This quantity is shown as the dashed line in Fig. 11; clearly the assumption is valid. If the line is fitted to a constant, we find that $[D(z)/n_\infty]e^{\beta W(z)}=(1.37\pm 0.10)\times 10^{-8}$ m^2 s^{-1}. Note that the results of this section were all obtained from simulations using sparse matrices; we have checked that the results are not significantly different when we use the full matrices.

The permeability P' as defined in Sec. II A can now be calculated. As is clear from Eqs. (2.4) and (2.5) the intrinsic permeability will be inversely proportional to the thickness of the material and independent of the area, as is expected from a resistor network analogy. By calculating the permeability of a single channel in a single unit cell, $P_{channel}$, it is straightforward to obtain the macroscopic permeability. For Theta-1 we find that

$$\frac{P'}{n_\infty e^{\beta W_{\text{Bulk}}}}=3.035\times 10^{13}\ \text{s/(m kg)},$$

where we have included the explicit correction associated with the free energy of the guest in the adjacent phases, W_{Bulk}, since the potentials used here have their zero defined relative to vacuum.

The diffusion of xenon in Theta-1 has not yet been studied experimentally. However, as mentioned above, Kärger *et al.* [40] examined the self-diffusion of xenon in silicalite. The high-temperature limit self-diffusion coefficient that they obtain with Eq. (4.8) is $D_o=(0.9\pm 0.2)\times 10^8$ m^2 s^{-1}. This can be compared with our value, i.e., $[D(z)/n_\infty]e^{\beta W(z)}=(1.37\pm 0.10)\times 10^{-8}$ m^2 s^{-1}, which, given the differences between the two systems and the quantities measured or calculated, is in reasonable agreement with the experimental value. In the next section, we discuss transition state theory within the context of the current approach.

V. TRANSITION STATE THEORY

Another approach that one could have used in order to get the permeability of the system is transition state theory (see, e.g., Ref. [43]). This theory treats the motion of the guest between two neighboring binding sites as an activated hopping process, where the kinetics are described by hopping rate constants that are fully determined by motion near the steepest descent path linking two binding sites. We found two types of saddle points (transition states) for our potential of mean force. Their corresponding steepest descent paths are shown in Fig. 5. The assumptions behind transition state theory are that there is an equilibrium between the reactants and the transition state and that there are no recrossings. Also, transition state theory will be accurate only if the average motion of the guest inside the crystal follows the reaction coordinates associated with each transition state. This last assumption can be verified in the following way.

If we start an ensemble of trajectories at the saddle point, we should see that, on the average, the guest moves to one of the two binding sites following the prescribed path. We started trajectories at the two saddle points (each ensemble

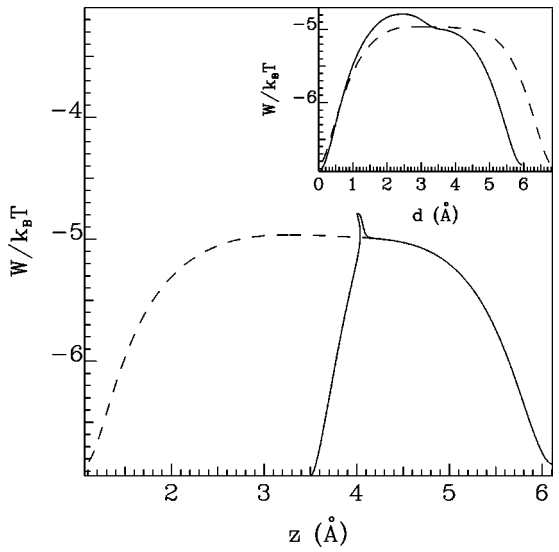

FIG. 6. The potential of mean force along path 1 (dashed line) and path 2 (full line). The energy is plotted as a function of z (and as a function of the distance d along the path in the inset). The activation energy for path 1 is $1.95k_BT$ and, for path 2, $2.15k_BT$ or $2.06k_BT$ (depending on the starting point) at 300 K.

contained 2000 members) and we averaged the trajectories conditional on which binding sites they end up in. The results are shown as 3D plots in Fig. 12, and clearly show from the average paths are qualitatively different than the steepest descent path. Moreover, while many of the trajectories that are started at a saddle point end up in the nearest neighbor minima, a significant fraction of trajectories also end up further away on the time scale of the velocity correlation function; for cases shown in Figs. 12(a) and 12(b), only 66.5% and 66.7%, at 300 K (blue curve), of the population is accounted for by those that end up in the nearest neighbor sites, respectively. In either example shown in Figs. 12(a) and 12(b), the short-time behavior of the average trajectories that do end up in the minima predicted by the minimum energy path is very different from the behavior expected from the steepest descent path.

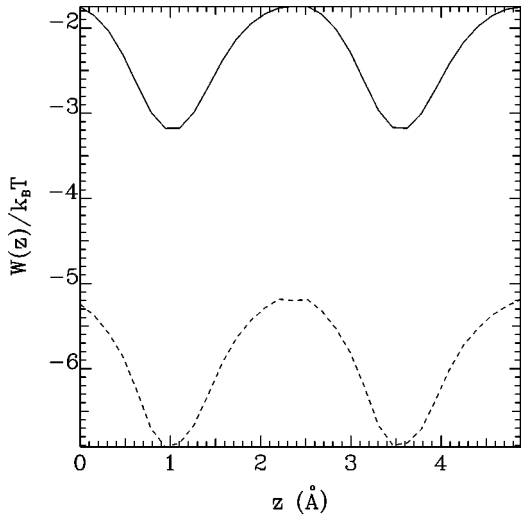

FIG. 7. The plane potential of mean force for the middle unit cell of the channel is represented by the full curve. The dashed curve shows the value of the minimum in every plane.

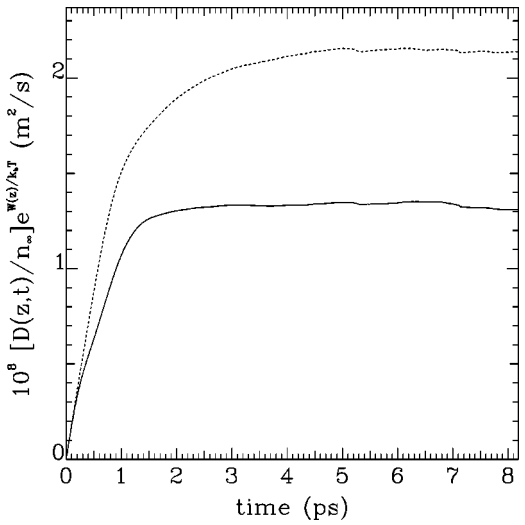

FIG. 8. $[D(z)/n_\infty]e^{W(z)/k_BT}$ for $z=2.519$ Å is extrapolated from the plateau value of the full line. The dashed line is the uncorrected result. This plane is a maximum energy plane, with respect to $W(z)$.

For the minimum energy path linking binding sites on the same side of the channel, the potential energy in the saddle plane suggests that trajectories that are directed away from the center along y will be backscattered towards the center of the channel. For the other saddle plane, it is now the trajectories that are initially aimed away from the center in x that will be backscattered towards the center. The xy components of the average trajectories for path 1 are plotted in Fig. 13 against their z component to emphasize the differences with the steepest descent path and illustrate the last comments. The error bars in these figures show that the steepest descent path is within the standard deviation associated with the av-

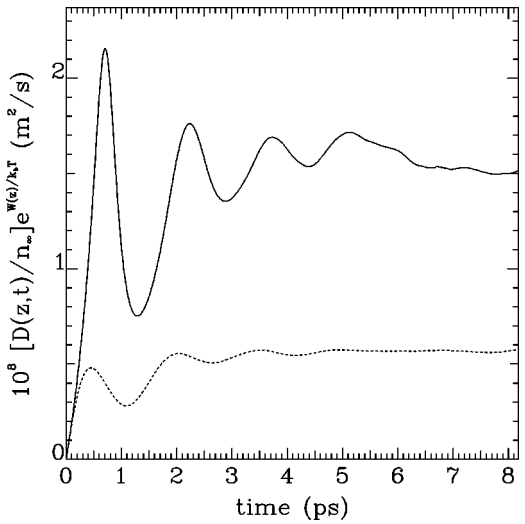

FIG. 9. $[D(z)/n_\infty]e^{W(z)/k_BT}$ for $z=0.944\,625$ Å is extrapolated from the plateau value of the full line. The dashed line is the uncorrected result. This plane is a minimum energy plane with respect to $W(z)$.

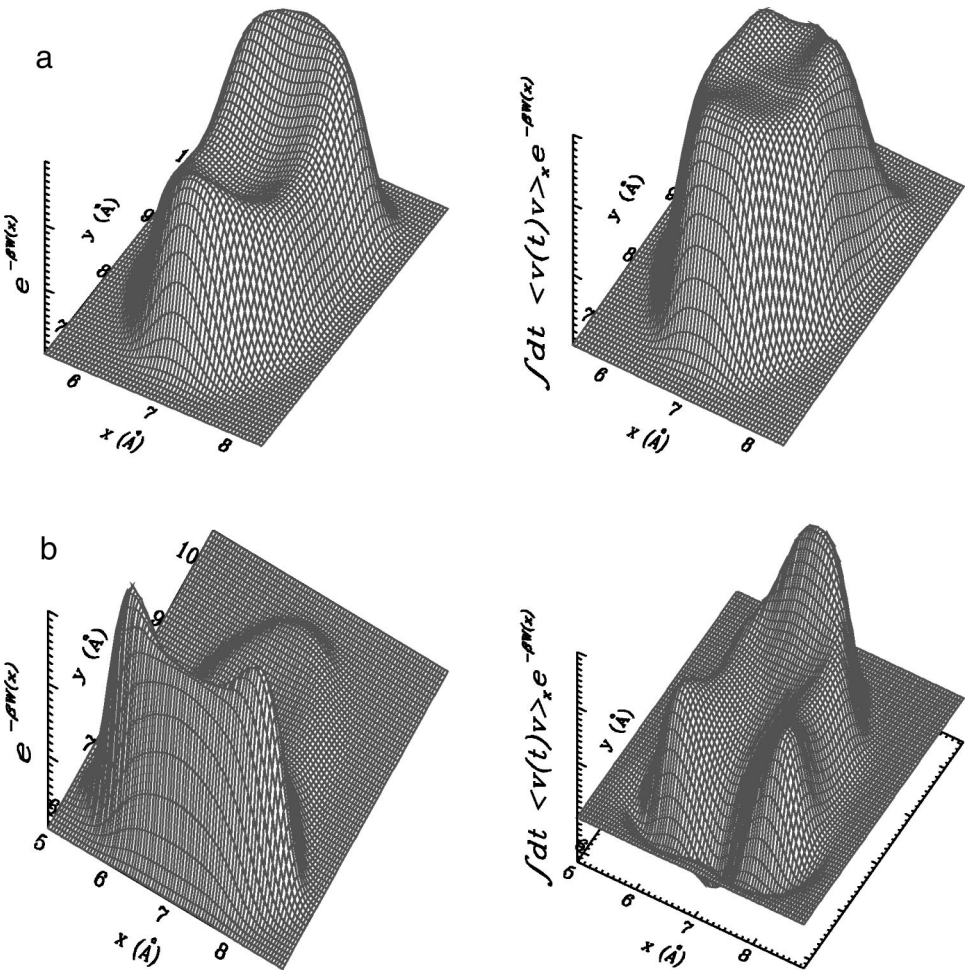

FIG. 10. The Boltzmann factor $e^{-W(\mathbf{r})/k_BT}$ and the factor $\int_0^\infty dt\langle v_z(t)v_z\rangle_{\mathbf{r}_\parallel}e^{-W(\mathbf{r})/k_BT}$ in the maximum (a) and minimum (b) $W(z)$ planes. The z axis has arbitrary units.

erage of the trajectories, but it is clear that the steepest descent paths alone do not accurately describe the dynamics.

Another way to verify the validity of transition state theory is to look at the parameter $\int dt\langle v_z(t)v_z\rangle_{\mathbf{r}}e^{-W(\mathbf{r})/k_BT}$ in the transition planes, as shown in Fig. 14. For transition state theory to be right, the plane averages in Eq. (4.9) must be dominated by the value of $\int dt\langle v_z(t)v_z\rangle_{\mathbf{r}}e^{-W(\mathbf{r})/k_BT}$ along the reaction coordinates. Hence, we expect a spike at the saddle point in the saddle planes. It is clear from these figures (the saddle point is indicated by an "*X*" in each plane) that the transition state contributes to the plane average, but that the rest cannot be neglected. Figure 14 shows that the saddle point gives the largest contribution while in saddle plane 2, the saddle point is not even the point with the largest contribution. We conclude that for this particular temperature (300 K), transition state theory does not properly describe the average motion of xenon in Theta-1. Our potential, which is very flat, is probably one of the reasons for this breakdown of transition state theory.

If the flatness of the potential is the main reason why transition state theory breaks down for our system, it is interesting to investigate the effects of reducing the temperature on the dynamics. The conditional average trajectories starting at the two saddle points at 3 K are shown in Figs. 12(a) and 12(b) as the green curves. These curves represent 86.8% and 98.6% of the populations for trajectories started at the saddle points 1 and 2, respectively. As expected, at least for path 1, the trajectories follow the steepest descent paths more closely at lower temperature.

For the path 2 saddle point, the average trajectory still

TABLE V. The diffusion coefficient in different planes.

Name	z (Å)	$[D(z)/n_\infty]\times 10^8$ m^{2}s^{-1}	$e^{-\beta W(z)}$	$[D(z)/n_\infty]e^{\beta W(z)}\times 10^8$ m^{2}s^{-1}
Minimum $W(z)$ plane	0.944625	38.11	24.05	1.5844
Saddle plane path 2	1.48	16.73	13.09	1.2782
Intermediate plane 1	1.57438	14.83	10.85	1.3669
Intermediate plane 2	2.36156	7.38	5.75	1.2847
Maximum $W(z)$ plane	2.519	7.67	5.74	1.3349
Saddle plane path 1	3.27	25.22	18.03	1.3988

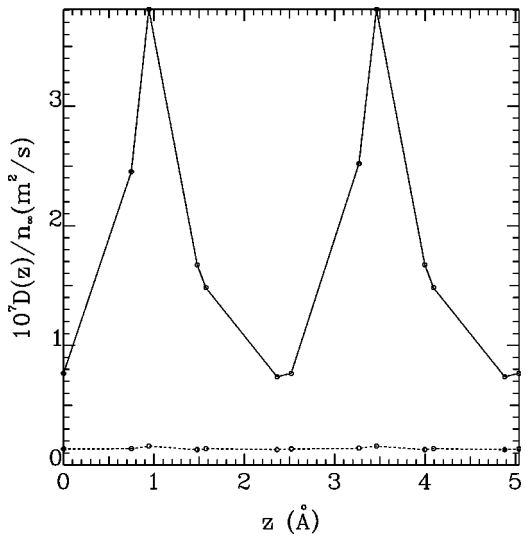

FIG. 11. The space-dependent diffusion coefficient $D(z)/n_\infty$ (solid line) and $[D(z)/n_\infty]e^{W(z)/k_BT}$ (dashed line).

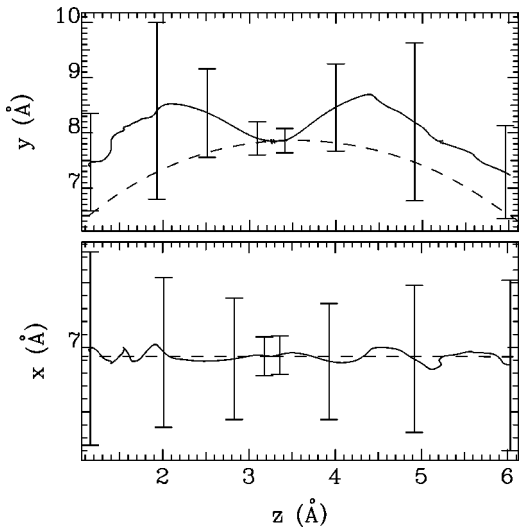

FIG. 13. The x and y components of the steepest descent path 1 (dashed line) and the average trajectory (full line). The starting point is at (6.9295 Å, 7.8445 Å, 3.27 Å). The average x component has to follow the reaction coordinate because it lies in the reflection plane. The errors bars indicate the standard deviation associated with the average.

does not follow the steepest path as well as it did for path 1 at low temperature. This happens for two reasons. First, in the region where path 2 merges into path 1, the steepest descent (path 2) bends sharply and the guest jumps out of steepest descent region, using the kinetic energy it has picked up in moving down the barrier. Second, the binding pocket has its two absolute minima on either side of the x-reflection plane in the unit cell, and the barrier separating them is extremely small compared to the kinetic energy picked up down the barrier; hence, the forces are not large enough to keep the guest localized near the ends of the steepest descent curve.

In a hopping model that incorporates hops along paths 1 and 2 and assumes fast equilibrium between the three binding sites in each of the low energy pockets, the steady-state flux is given by

$$J = -\frac{2\rho_c K_{eq}(k_1 K_\perp + 2k_2)}{(2K_\perp + 1)Nn_\infty k_B T}(\mu_+ - \mu_-), \tag{5.1}$$

where k_i is the rate constant associated with path i, N is the number of binding pockets in one channel (assumed large), ρ_c is the number of channels per unit area, and the equilibrium constants K_{eq} and $K_\perp$ govern the equilibrium between the bulk and the first binding pocket or that between the three binding sites within a pocket, respectively. Finally, we have used the linear approximation $\delta\mu_\pm \sim k_B T \delta n_\pm / n_\infty$.

Transition state theory makes an unambiguous prediction for the hopping rate constants k_1 and k_2 [44]. By assuming that K_{eq} can be obtained from a Langmuir adsorption model where bulk atoms are absorbed onto a surface (the first binding planes in the crystal), we find that

$$\frac{2k_1 K_\perp K_{eq}}{2K_\perp + 1} = 2\left(\frac{2\pi(k_B T)^3}{m_G K_\eta^{(1)} K_\zeta^{(1)}}\right)^{1/2} e^{-\beta(W_1^\ddagger - W_{bulk})} \tag{5.2}$$

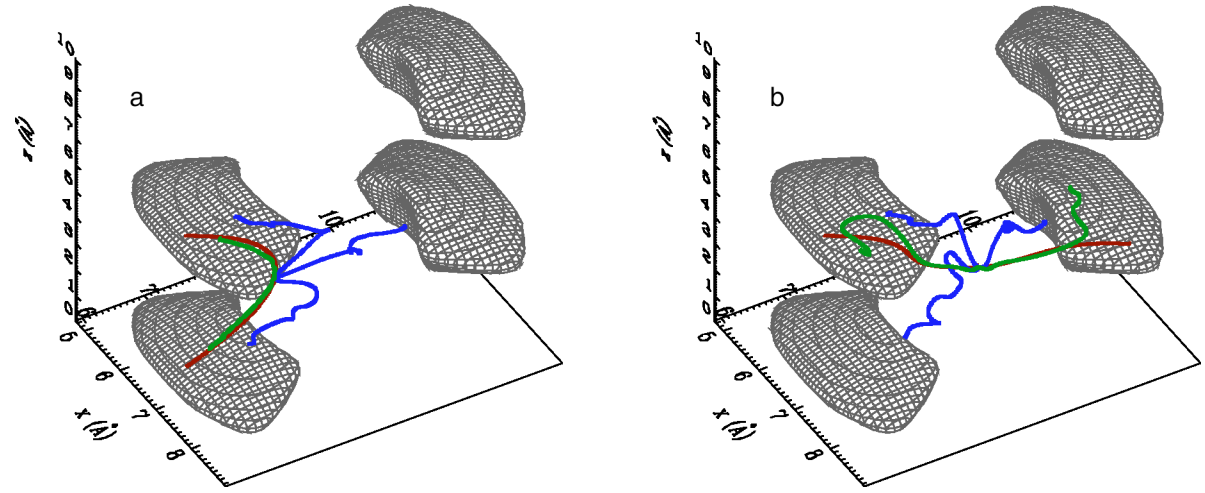

FIG. 12. (Color online) The steepest descent path 1 (a), and the steepest descent path 2 (b) (in red) are compared with the conditional averages of the trajectories started at the appropriate saddle point at 300 K (blue) and 3 K (green). The surface is at $-5.3k_BT$.

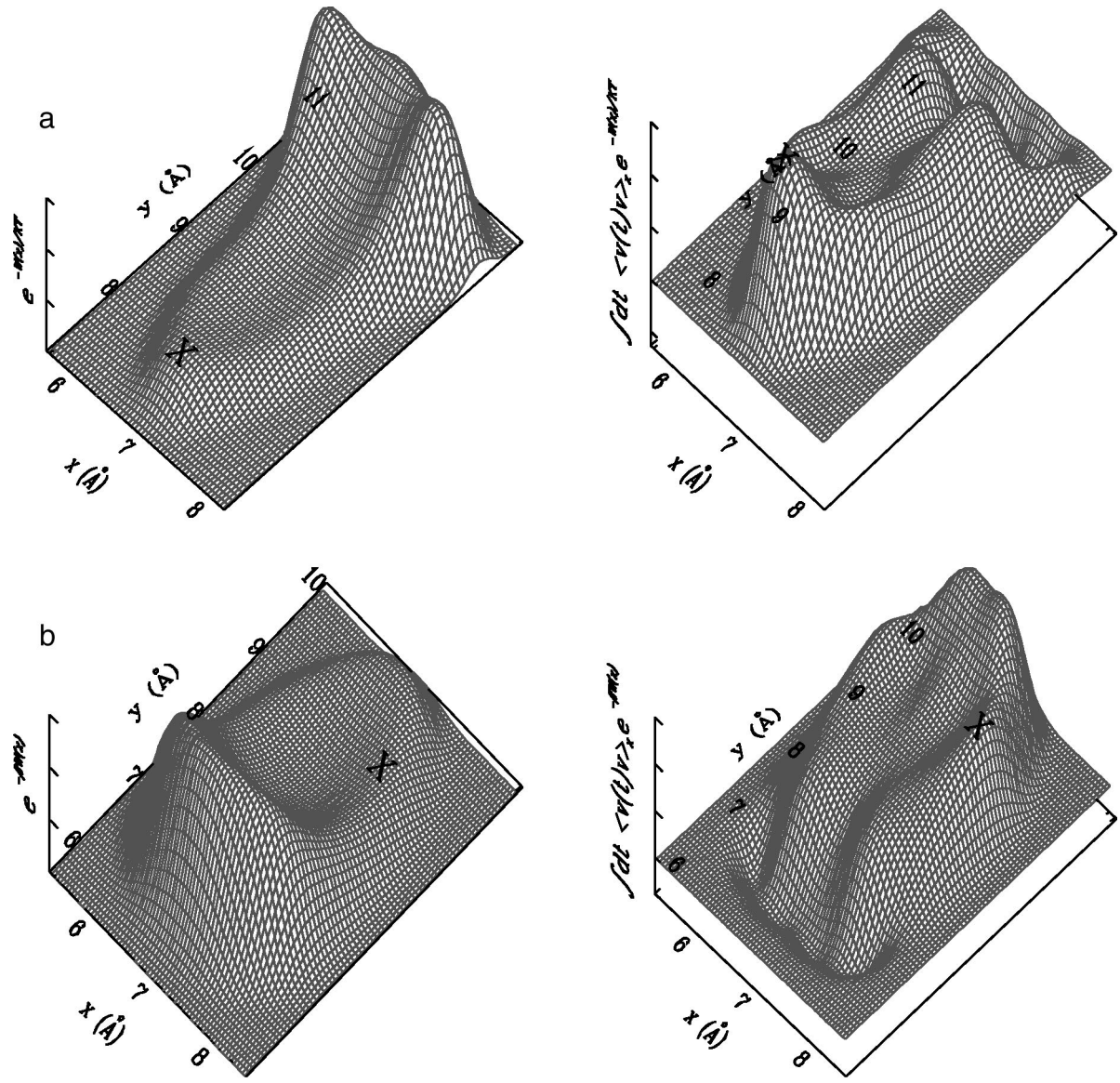

FIG. 14. The Boltzmann factor $e^{-W(\mathbf{r})/k_BT}$ and the factor $\int_0^\infty dt\langle v_z(t)v_z\rangle_{\mathbf{r}_\parallel} e^{-W(\mathbf{r})/k_BT}$ in saddle plane 1 (a) and saddle plane 2 (b). The z axis has arbitrary units.

and

$$\frac{4k_2K_{eq}}{2K_\perp+1}=4\left(\frac{2\pi(k_BT)^3}{m_GK_\eta^{(2)}K_\zeta^{(2)}}\right)^{1/2}e^{-\beta(W_2^\ddagger-W_{bulk})}, \quad (5.3)$$

where $W_i^\ddagger$ and the $K_{\eta,\zeta}^{(i)}$'s are the energy and vibrational force constants for motion transverse to the steepest descent path at the ith saddle point, respectively. In writing Eqs. (5.2) and (5.3) we have ignored the vibrational motion of the lattice, other than in its contribution to $W_{1,2}^\ddagger$, treated the guest vibrations classically, and have assumed a unit transmission coefficient.

By using Eqs. (5.2) and (5.3) for the saddle points and paths shown in Fig. 5 in Eq. (5.1), we obtain

$$\frac{P_{\mathrm{TST}}{}'}{n_\infty e^{\beta W_{\mathrm{Bulk}}}}=5.439\times10^{13}\ \mathrm{s/(m\,kg)},$$

which is clearly different from the value obtained with our method. While part of the difference could be blamed on our use of high-temperature, harmonic, partition functions for the vibrational motion transverse to the reaction coordinate in the transition state approach, it is clear that the basic assumptions of the transition state theory are not satisfied very well, as was discussed above.

In fact, the large contribution to the permeability from regions other than the steepest descent lines manifests itself in other ways. For example, if we define an apparent activation energy as $\Delta E^\ddagger\equiv\partial\ln P/\partial(-\beta)$, we find that, at 300 K, $\beta\Delta E_{\mathrm{TST}}^\ddagger=-4.38$, compared with $\beta\Delta E^\ddagger=-2.48$ using our method. In both cases, the number is reported with respect to

the bulk energy, and in our method, we have ignored the temperature dependence of $D(z)e^{\beta W(z)}$.

VI. CONCLUDING REMARKS

One important result of this work is that $D(z)e^{\beta W(z)}$ is not only constant in the vicinity of the barrier tops, it is roughly constant throughout the channel for our system. This means that the diffusion of xenon in Theta-1 is well described as a Smoluchowski [24] process, which says that $D(z) \propto e^{-\beta W(z)}$, and, as we saw above, not by transition state theory.

Our expression for the potential of mean force, Eq. (3.40), includes the relaxation of the lattice and a temperature correction term. It is a common practice to neglect both of these effects. For example, experimental evaluation of diffusion in silicates (see, e.g., Ref. [45]), often assumes that the activation energy is temperature independent. Also, a rigid lattice is often used in simulations and in the calculation of the available volume for a guest inside a zeolite (see, e.g., Ref. [35]). We have verified that neglecting the temperature dependence of the potential of mean force does not lead to large errors. The use of a rigid lattice leads to larger, but still acceptable, errors on the shape of the potential for the system investigated. There is a more important problem associated with the dynamical studies of a guest in a channeled structure using a rigid lattice which is that the lattice cannot dissipate the guest's energy—especially when the activation energy is large.

We computed velocity correlation functions at some test points using a rigid lattice, and it turns out that these are similar to the ones that are obtained with flexible lattice. The decay of the velocity correlation functions occur on the same time scale in both cases, and in the rigid lattice arises solely because of the dephasing associated with the average over initial velocities (kinetic energy correlations are quite different). There are two main mechanisms leading to the decay of the velocity correlation functions. The first is the randomization of the direction of $\mathbf{v}_G(t)$. The second arises from the fact that total energy of the guest is not conserved in a flexible lattice and this manifests itself in the magnitude of the guest velocity. For our system, the energy exchange between the guest and the lattice occurs on a somewhat longer time scale compared to that associated with randomization of the direction, and thus, this latter effect is captured by the rigid lattice calculations at short and intermediate times.

On the other hand, the relaxation of the lattice will have bigger effects on the shape of the potential in small crystal structures (i.e., β-quartz) where the guest is often in the strongly repulsive part of the pair potential, where the energies are larger, and where lattice distortions are larger. In addition, anharmonicities and energy exchange will be more important.

In this work, we used generalized Langevin equations to simulate the target equations of motion. It is clear from Secs. II A and II B that the evaluation of the macroscopic permeability can be obtained from standard MD. We opted for the GLE approach because the consistency of our method relies, in part, in the accurate description of the infinite crystal vibrations. In MD this is achieved when the number of simulated atoms is large. Using GLE's allows us to drastically reduce the number of simulated degrees of freedom .

Note that the macroscopic permeability of the Theta-1 interface may be hard to get experimentally. In fact, Theta-1 crystals are usually needlelike crystallites with length ranging from 0.6–1.0 μm and width from 0.06–0.10 μm [2]. It may therefore be difficult to construct a macroscopic interface where all the channels are aligned. Also, as noted by Kärger *et al.* [4] in their work on single-file diffusion, 1D channels can easily be blocked, and hence, in an experiment, not all channel will participate in the transport, thereby giving a lower apparent single-channel permeability.

In conclusion, we briefly summarize the main features of our approach. First, we believe that our theory is well suited for diffusion studies in systems containing large potential barriers where hopping events are rare, and moreover, does not make *a priori* assumptions about steepest descent paths (and which turn out to be unwarranted for the example considered here). Second, the Langevin equation is exact to the extent that the guest does not interact directly with the target, that all the forces within the crystal are harmonic, and the vibrational density of states of the full crystal is accurately reproduced by our approximation for the force-force time correlation function. This leads to a practical simulation that incorporates the full vibrational motion of the crystal. In addition, the required time correlation functions are obtained on a ps time scale.

Third, we introduced an accurate and simple way of obtaining the guest potential of mean force for the system and we tested it against the simulation results.

Fourth, the expression for $D(z)$, cf. Eq. (2.5) which requires the evaluation of plane averages is general and can be applied to any crystal system with connected channels. With such a system the guest is allowed to travel in different channels and the simulations might have to be performed over larger extents of the full crystal. This would make the problem more difficult numerically. In addition, some assumptions about the range of the correlations that appear in the memory functions in Eq. (1.4) made in obtaining the expression for the permeability in Ref. [15] might break down if the structure is too porous and does not contain solvent.

Finally, we have seen that transition state theory gives a very different prediction at room temperatures in Theta-1, in part due to the very anharmonic nature of the potentials, and in particular, due to the contribution of other regions of the channel to the permeability.

In a subsequent paper, we will investigate the diffusion of noble gases in β-quartz where the energy barriers are large. For such a system, the flexibility of the lattice plays a crucial role. On the other hand, transition state theory is expected to be more accurate. Another interesting aspect would be to investigate the role of quantum mechanics in our analysis.

ACKNOWLEDGMENTS

We would like to thank the Natural Sciences and Engineering Research Council of Canada for supporting this

work. One of us (B.P.) also thanks the Fonds de recherche sur la nature et les technologies of Quebec for support.

APPENDIX A: EQUATIONS OF MOTION

In this appendix, we demonstrate that $-\dot{\mathsf{y}}(t)$ replaces the noise and memory term in Eq. (2.7). In what follows, the T subscript will be omitted for matrices and vectors in the target space. We rewrite Eq. (3.32) as

$$\dot{\mathsf{Y}}(t) = -\bar{\mathsf{M}}\mathsf{Y}(t) + \mathsf{N}(t) + \mathsf{P}'(t), \tag{A1}$$

where

$$\mathsf{Y}(t) \equiv \begin{pmatrix} \mathsf{y}(t) \\ \dot{\mathsf{y}}(t) \end{pmatrix}, \tag{A2a}$$

$$\mathsf{N}(t) \equiv \begin{pmatrix} 0 \\ \mathsf{C}^{-1}\boldsymbol{\eta}(t) \end{pmatrix}, \tag{A2b}$$

$$\mathsf{P}'(t) \equiv \begin{pmatrix} 0 \\ \mathsf{C}^{-1}\mathsf{M}^{-1}\mathsf{P}(t) \end{pmatrix}, \tag{A2c}$$

and

$$\bar{\mathsf{M}} \equiv \begin{pmatrix} 0 & -1 \\ \mathsf{C}^{-1}\mathsf{A} & \mathsf{C}^{-1}\mathsf{B} \end{pmatrix}, \tag{A2d}$$

where each block of $\bar{\mathsf{M}}$ is a square matrix. The formal solution of Eq. (A1) is

$$\mathsf{Y}(t) = e^{-\bar{\mathsf{M}}t}\mathsf{Y}(0) + \int_0^t dt_1 e^{-\bar{\mathsf{M}}(t-t_1)}\mathsf{N}(t_1) + \int_0^t dt_1 e^{-\bar{\mathsf{M}}(t-t_1)}\mathsf{P}'(t_1). \tag{A3}$$

The last term of this equation is very similar to the memory term in our Langevin equation, Eq. (2.7), and, in fact, it contains that term. Since the last term is a convolution, when Laplace transformed, it becomes

$$(\bar{\mathsf{M}} + s)^{-1}\mathsf{P}'(s).$$

If we keep in mind that the upper half part of P' is zero (the first $3N_{\text{Target}}$ elements) and if we denote the inverse as

$$(\bar{\mathsf{M}} + s)^{-1} \equiv Q(s) \equiv \begin{pmatrix} q_{11} & q_{12} \\ q_{21} & q_{22} \end{pmatrix}, \tag{A4}$$

then only the 12 and the 22 parts of the inverse will contribute. Evaluating the inverse, we find that

$$q_{12} = -\frac{1}{\mathsf{A} + \mathsf{B}s + \mathsf{C}s^2}\mathsf{A} \tag{A5}$$

and

$$q_{22} = \frac{s}{\mathsf{A} + \mathsf{B}s + \mathsf{C}s^2}\mathsf{C}, \tag{A6}$$

which when multiplied by $\mathsf{C}^{-1}\mathsf{M}^{-1}\mathsf{P}(s)$, shows that $q_{22}\mathsf{C}^{-1}\mathsf{M}^{-1}\mathsf{P}$ gives the expected term, i.e.,

$$q_{22}\mathsf{C}^{-1}\mathsf{M}^{-1}\mathsf{P} = \frac{s}{\mathsf{A} + \mathsf{B}s + \mathsf{C}s^2}\mathsf{M}^{-1}\mathsf{P}(s),$$

and hence, to the accuracy of our approximate representation of the memory function, Eq. (3.27),

$$\mathsf{Y}_2(t) \approx \left[e^{-\bar{\mathsf{M}}t}\mathsf{Y}(0) + \int_0^t dt_1 e^{-\bar{\mathsf{M}}(t-t_1)}\mathsf{N}(t_1) \right]_2 + \beta \int_0^t dt_1 \langle \mathsf{F}_T^{\dagger}(t-t_1)\mathsf{F}_T^{\dagger T} \rangle \mathsf{M}^{-1}\mathsf{P}(t_1), \tag{A7}$$

where the subscript 2 refers to the lower half of the column vectors. Therefore, in order to include friction in the equations of motion, we will need to subtract the second part of $\mathsf{Y}(t)$ from the equations for $\dot{\mathsf{P}}(t)$. This is indeed done in Eq. (3.31).

The $\mathsf{Y}(t)$ must also describe the random force [cf. Eq. (2.7)] through the white noise term. From Eq. (A7) and from Eq. (2.7), it is clear that the random force $\mathsf{F}^{\dagger}(t)$ should be represented by

$$\mathsf{F}^{\dagger}(t) = \left[e^{-\bar{\mathsf{M}}t}\mathsf{Y}(0) + \int_0^t dt_1 e^{-\bar{\mathsf{M}}(t-t_1)}\mathsf{N}(t_1) \right]_2. \tag{A8}$$

A few manipulations show that this is indeed the case if

$$\langle \mathsf{N}\mathsf{N}^T \rangle = \begin{pmatrix} 0 & 0 \\ 0 & k_B T \mathsf{C}^{-1}\mathsf{B}\mathsf{C}^{-1} \end{pmatrix}, \tag{A9}$$

and if the random initial conditions for Y satisfy

$$\langle \mathsf{Y}_1 \mathsf{Y}_1^T \rangle = k_B T \mathsf{A}^{-1} \tag{A10}$$

and

$$\langle \mathsf{Y}_2 \mathsf{Y}_2^T \rangle = k_B T \mathsf{C}^{-1}, \tag{A11}$$

where the averages of $\mathsf{N}(t)$, Y_1, and Y_2 are zero.

APPENDIX B: ENERGY COST OF A LOCAL DISPLACEMENT IN AN ELASTIC MEDIUM

This appendix discusses the energy cost for a local displacement in an infinite isotropic continuum. As shown in Ref. [46], the vector field **u** describing the displacement of the continuum lattice at position r obeys the equation

$$(1-2\sigma)\nabla^2 \mathbf{u}(\mathbf{r}) + \nabla[\boldsymbol{\nabla} \cdot \mathbf{u}(\mathbf{r})] = 0, \tag{B1}$$

where σ is Poisson's ratio. The free energy cost per unit volume is given by,

$$E=\mu(u_{ik}-\tfrac{1}{3}\delta_{ik}u_{ll})^2+\tfrac{1}{2}\kappa u_{ll}^2, \tag{B2}$$

where summation over repeated indices is implied. The quantities κ and μ are the bulk modulus and the modulus of compression, respectively, and the elements of the symmetric strain tensor u_{ik} are given by

$$u_{ik}=\frac{\partial u_i(\mathbf{r})}{\partial r_k}+\frac{\partial u_k(\mathbf{r})}{\partial r_i}. \tag{B3}$$

To get the full energy of the system, Eq. (B2) is integrated over the whole system.

For the case of interest, the following boundary conditions will apply in d dimensions:

$$\mathbf{u}(r,\Omega)=0 \text{ as } r\to\infty, \tag{B4a}$$

$$\mathbf{u}(a,\Omega)=\delta\mathbf{u}, \tag{B4b}$$

where Ω represents the angular coordinates. The boundary condition at infinity comes from tethering the edges of the lattice, while that at $r=a$ represents, for our problem, a uniform displacement of the target zone along an arbitrary axis. We solved this problem in one, two, and three spatial dimensions using the following *ansatz*:

$$\mathbf{u}(\mathbf{r})=\boldsymbol{\nabla}\phi(\mathbf{r})+\boldsymbol{\nabla}\times\mathbf{A}(\mathbf{r}). \tag{B5}$$

Since we are using linear elasticity, these potentials must have forms

$$\phi(\mathbf{r})=\delta\mathbf{u}\cdot\mathbf{r}f(r) \tag{B6}$$

and

$$\mathbf{A}(\mathbf{r})=\delta\mathbf{u}\times\mathbf{r}g(r). \tag{B7}$$

The boundary conditions are then expressed in terms of the f and g functions, the differential equation is solved and the energy cost for such a local displacement is computed. We found that there was zero energy cost in one or two spatial dimensions, while in three dimensions it becomes

$$E=6\pi\mu\frac{3\kappa+4\mu}{6\kappa+11\mu}\delta u^2 a. \tag{B8}$$

For typical values of the moduli and a, this energy is large compared with k_BT, thereby confirming our hypothesis that the channel cannot uniformly translate to reduce its energy.

[1] J. Käger and D. M. Ruthven, *Diffusion in Zeolites and Other Microporous Materials* (Wiley, New York, 1992).
[2] F. Geobaldo, S. Fiorilli, B. Onida, G. Giordano, A. Katovic, and E. Garrone, J. Phys. Chem. B **107**, 1258 (2003).
[3] J. Kärger, M. Petzold, H. Pfeifer, S. Ernst, and Jens Weitkamp, J. Catal. **136**, 283 (1992).
[4] K. Hahn, J. Kärger, and V. Kukla, Phys. Rev. Lett. **76**, 2762 (1996).
[5] R.M. Barrer and D.L. Peterson, Proc. R. Soc. London, Ser. A **280**, 466 (1964).
[6] G.D. Mayorga and D.L. Perterson, J. Phys. Chem. **76**, 1641 (1972).
[7] V. Mehra, R. Basra, M. Khanna, and C. Chakravarty, J. Phys. Chem. B **103**, 2740 (1999).
[8] S. El Amrani, F. Vigné-Maeder, and B. Bigot, J. Phys. Chem. **96**, 9417 (1992).
[9] Anastasios I. Skoulidas and David S. Scholl, J. Phys. Chem. B **106**, 5058 (2002).
[10] T. Mosell, G. Schrimpf, C. Hahn, and J. Brickmann, J. Phys. Chem. **100**, 4571 (1996).
[11] T. Mosell, Ge. Schrimpf, and J. Brickmann, J. Phys. Chem. **100**, 4582 (1996).
[12] T. Mosell, G. Schrimpf, and J. Brickmann, J. Phys. Chem. B **101**, 9476 (1997).
[13] H. Mori, Prog. Theor. Phys. **34**, 423 (1965).
[14] R. Zwanzig, *Lectures in Theoretical Physics* (Interscience, New York, 1961), Vol. 3.
[15] M. Vertenstein and D. Ronis, J. Chem. Phys. **85**, 1628 (1986).
[16] G. Schrimpf, M. Schlenkrich, J. Brickmann, and P. Bopp, J. Phys. Chem. **96**, 7404 (1992).
[17] D.I. Kopelevich and H.-C. Chang, J. Chem. Phys. **114**, 3776 (2001). Unlike in this work, Kopelevitch and Chang use a highly simplified, *ad hoc*, model for the random force correlation function.
[18] M. Vertenstein and D. Ronis, J. Chem. Phys. **87**, 5457 (1987).
[19] J.M. Deutch and R. Silbey, Phys. Rev. A **3**, 2049 (1971).
[20] J.C. Tully, J. Chem. Phys. **73**, 1975 (1980).
[21] A.C. Diebold, S.A. Adelman, and C.Y. Mou, J. Chem. Phys. **71**, 3236 (1979).
[22] A. A. Maradudin, I. M. Lifshitz, A. M. Kosevitch, W. Cochran, and M. J. P. Musgrave, *Lattice Dynamics* (Benjamin, New York, 1969).
[23] M. Born and K. Huang, *Dynamical Theory of Crystal Dynamics* (Oxford University Press, Oxford, 1968).
[24] N. Wax, *Selected Papers on Noise and Stochastic Processes* (Dover, New York, 1954).
[25] R. Kubo, Proc. Phys. Soc. Jpn. **17**, 1100 (1962).
[26] N.D. Mermin and H. Wagner, Phys. Rev. Lett. **17**, 1133 (1966); N.D. Mermin, Phys. Rev. **176**, 250 (1968).
[27] R.M. Highcock, G.W. Smith, and D. Wood, Acta Crystallogr., Sect. C: Cryst. Struct. Commun. **41**, 1391 (1985).
[28] M.W. Deem, J.M. Newsam, and J.A. Creighton, J. Am. Chem. Soc. **114**, 7198 (1992).
[29] B.W.H. van Beest, G.J. Kramer, and R.A. van Santen, Phys. Rev. Lett. **64**, 1955 (1990).
[30] S. Tsuneyuki, M. Tsukada, H. Aoki, and Y. Matsui, Phys. Rev. Lett. **61**, 869 (1988).
[31] F. London, Z. Phys. Chem. Abt. B **11**, 222 (1930).
[32] J.G. Kirkwood, Phys. Z. **33**, 57 (1932).
[33] H.R. Muller, Proc. R. Soc. London, Ser. A **154**, 624 (1936).
[34] A.V. Kiselev and P.Q. Du, J. Chem. Soc., Faraday Trans. **77**, 1 (1981).

[35] D. Keffer, V. Gupta, D. Kim, E. Lenz, H.T. Davis, and A.V. McCormick, J. Mol. Graphics **14**, 108 (1996).
[36] http://www.hbcpnetbase.com/.
[37] A. Bondi, J. Phys. Chem. **68**, 441 (1964).
[38] J. O. Hirshfelder, C. F. Curtiss, and R. B. Bird, *Molecular Theory of Gases and Liquids* (Wiley, New York, 1954).
[39] S. Kar and C. Chakravarty, Mol. Phys. **99**, 1517 (2001).
[40] J. Kärger, H. Pfeiffer, F. Stallmach, N.N. Feoktistova, and S.P. Zhdanov, Zeolites **13**, 50 (1993).
[41] http://math.nist.gov/spblas/
[42] P. E. Kloeden, E. Platen, and H. Schurz, *Numerical Solutions of SDE Through Computer Experiments* (Springer-Verlag, Berlin, 1994).
[43] H. Eyring, J. Chem. Phys. **3**, 107 (1935).
[44] See, e. g., T. L. Hill, *An Introduction to Statistical Thermodynamics* (Dover, New York, 1986), Sec. 11-3.
[45] R. M. Barrer, *Diffusion in and through Solids* (Cambridge University Press, New York, 1941).
[46] L. D. Landau and E. M. Lifshitz, *Theory of Elasticity* (Pergamon Press, New York, 1975).